Two-Dimensional Multi-Label Active Learning with An Efficient Online Adaptation Model for Image Classification

Guo-Jun Qi, Xian-Sheng Hua, *Member, IEEE,* Yong Rui, *Senior Member, IEEE,*
Jinhui Tang, *Student Member, IEEE* and Hong-Jiang Zhang, *Fellow, IEEE*

Abstract— **Conventional active learning dynamically constructs the training set only along the sample dimension. While this is the right strategy in binary classification, it is sub-optimal for multi-label image classification. We argue that for each selected sample, only some effective labels need to be annotated while others can be inferred by exploring the label correlations. The reason is the contributions of different labels to minimizing the classification error are different due to the inherent label correlations. To this end, we propose to select sample-label pairs, rather than only samples, to minimize a multi-label Bayesian classification error bound. We call it two-dimensional active learning because it considers both the sample dimension and the label dimension. Furthermore because the number of training samples is increasing rapidly over time due to active learning, it becomes intractable for the offline learner to retrain a new model on the whole training set. So we develop an efficient online learner to adapt the existing model with the new one by minimizing their model distance under a set of multi-label constraints. The effectiveness and efficiency of the proposed method are evaluated on two benchmark datasets and a realistic image collection from a real-world image sharing website - Corbis.**

Index Terms— **Active learning, online adaption, multi-label classification, image annotation.**

I. Introduction

The goal of image classification is to assign a set of labels to images based on their semantic content. In most existing approaches, image classification has been formulated as either multi-class or multi-label problem. As multi-class problem, each image can be labeled by one and only one class. An example under such a classification setting is the Caltech 101 [1] annotation, in which each image in this data set is classified as only one object category. However in most real-world problems, multiple labels can be assigned to an image. For example, in many online image sharing websites (e.g., Flickr, Picasa, and Yahoo! Gallery), most of the images have more than one tags manually labeled by users. This classification setting results in a multi-label problem which is more complex and challenging compared to multi-class problem. In this paper, we will focus on image classification under this multi-label setting. Specifically, we will use active learning as the tool, and extend it from a one-dimensional sample-centric approach to a two-dimensional joint sample-label-centric approach for multi-label image classification. We further propose an online multi-label classification algorithm which can incrementally updates the classification model once new image samples are selected by the proposed active learning strategy. Such an online algorithm can avoid retraining the multi-label model so that it is computationally efficient to adapt the classifier to capture the semantic changes of the online image content.

In traditional classification scenarios [2] [3] [4], a batch of training images are first *statically* annotated by a set of semantic labels, and then they are used to train a classifier. However, in many online applications (e.g., the image sharing websites) users can *dynamically* upload new images, which have significant difference from the existing image collections due to the changes of the user-focuses and semantic "concept drift" in the low-level feature space. Moreover, these images can often be annotated by multiple labels simultaneously and it poses more challenges to handle these multi-label image sets. To deal with this online setting, traditional approaches are restricted by the following two problems:

- To adapt the existing classifier to the "concept" drift over time, we must manually collect the multi-label ground truth from the newly-acquired images. As well known, it is labor intensive and subject to annotation errors, especially when these image sets are large and need to annotate multiple labels for each image. In most cases, it is unnecessary to completely label all the new images and all their associated labels due to the fact that there exist redundancies between the different images. Therefore, we can design a strategy to utilize these redundancies to improve adaptation efficiency of the online models with only a small number of elaborately-selected samples.
- Once a set of images are collected together with their labeling ground truth, a direct solution to obtaining a new classifier is to retrain the classification model with

G.-J. Qi is with the Department of Automation, the University of Science and Technology of China, Hefei, Anhui 230027. E-mail: qgj@mail.ustc.edu.cn.

X.-S. Hua is with the Internet Media Group, Microsoft Research Asia, Beijing, Beijing 100080. E-mail: xshua@microsoft.com.

Y. Rui is with the Microsoft China R&D Group, Beijing, Beijing 100080. E-mail:yongrui@microsoft.com.

J. Tang is with the School of Computing, National University of Singapore, 119077, Singapore. E-mail: tangjh@comp.nus.edu.sg.

H.-J. Zhang is with Microsoft Advanced Technology Center, Beijing, Beijing 100080. E-mail:hjzhang@microsoft.com.

all the historical training set plus the newly-acquired images. However, the intensive computational cost has restricted many sophisticated models to be retrained in practice. So an efficient algorithm is desired to incrementally adapt the image models with the new images.

To handle the above issues, we propose an online two-dimensional active learning algorithm for multi-label image classification together with an efficient online adaptation model.

Active learning is one of the most widely-used approaches in image classification, as it can significantly reduce the effort in labeling training samples [5] [6] [7] [8]. Specifically, active learning approaches iteratively annotate a set of elaborately selected samples so that the expected classification error is minimized in each iteration. As a result, the total number of training samples that need to be labeled is smaller than non active learning approaches. The core of any active learning approach is the sample selection strategy. In the past decade, a number of active learning approaches were developed using different sample selection strategies [9] [10] [6]. For example, [11] [2] have explored reduction in uncertainty as the sample selection criterion and competitive performances have been achieved. Most of these approaches focus on the binary classification. However, in many real-world applications [12] [13] [3], a sample is usually associated with multiple labels rather than a single one. Under such a multi-label setting, each sample will be annotated as either "positive" or "negative" for each and every label. As a result, active learning with multi-label samples is much more challenging than that with binary-label ones, especially when the number of labels is large.

A direct way to tackle active learning under multi-label setting is to translate it into a set of binary problems, i.e., each category/label is independently handled by a binary active learning algorithm. For example, in [12] [14] two research groups have proposed such a binary-based active learning algorithm for multi-label classification problem, respectively. However, these approaches do not take into account the inherent relationship among multiple labels. In this paper, we propose a novel active learning strategy which iteratively selects sample-label pairs to minimize the expected classification error. Specifically, in each iteration, human annotators are only required to annotate/confirm a selected part of labels of selected samples while the remaining unlabeled part can be inferred according to the label correlations. We call this strategy 2 Dimensional Active Learning (2DAL) because it considers not only the samples to be labeled along the sample dimension but also the labels associated with these samples along the label dimension. An intuitive explanation of this strategy is that there exist both sample and label redundancies for multi-label samples. Therefore, annotating a set of selected sample-label pairs provides enough information for training the classifiers since the information in these pairs can be propagated to the rest along both the sample "dimension" and the label "dimension". Such a strategy significantly can reduce the required human labor. For example, "field" and "mountain" tend to occur simultaneously in an image. Therefore, it is reasonable to select only one label (e.g., "mountain") for annotation since the uncertainty of the other label can be remarkably decreased after annotating this one. Another example is "mountain" and "urban". In contrast to "field" and "mountain", these two labels often do not occur simultaneously. Thus, annotating one of them will probably eliminate the existence of the other one.

For the online applications, the second important issue is about an efficient online model-adaptation algorithm. With more and more new sample-label pairs are added into training set during the 2DAL procedure, the multi-label model must be updated accordingly. The most straightforward approach is to retrain the model on the whole training set. However, such an offline approach will become impractical when more and more samples come into the training set over time. On the other hand, as the semantic meanings of the image concepts are keeping changing due to the evolution of user focuses (e.g., users are keeping changing their attentions due to the evolution of the fashion and news) and photography techniques (e.g., film photography ten years before versus digital photographing today), a balance scheme should be incorporated into model adaptation algorithm so that it can trade off between the old knowledge preserved in the existing model and the new information contained in newly-acquired images. Thus, retraining the model with all old and new samples equally-weighted in a batch-mode manner is not a proper scheme, especially when the number of the new samples are much smaller than the number of the old ones. It probably underestimates the effect of new images.

In contrast to the naive retraining approach, we propose a novel online adaptation algorithm for multi-label image classification. It can directly update the existing model with the new samples rather than with the whole training images. Thus, it is much more efficient for model adaptation during the 2DAL procedure than the traditional retraining approach. Furthermore instead of equally using the old and new samples, this adaptation algorithm balances between preserving the old knowledge and complying with the new information. It can better leverage the new samples to capture evolution of concept semantics over time in many online applications. In particular, we formulate such an online adaptation algorithm by optimizing a variational problem which minimizes the distance between the new and old models under a set of multi-label constraints. Compared to the widely-used fully Bayesian approach [1] that requires to construct a set of intractable conjugate distributions, the model can be efficiently updated.

In brief, we summarize our contributions in this paper:

- We propose a novel two-dimensional active learning strategy for multi-label image classification. It actively selects sample-label pairs to minimize the expected Bayesian classification error bound. This strategy utilizes the rich label correlations so that the entire annotation labor can be dramatically reduced.
- In each active learning iteration, an efficient online adaptation algorithm is developed to update the multi-label model without the need of retraining with all historical training samples. It can also balance between the knowledge preserved in the old model and the information contained in newly-acquired samples, as

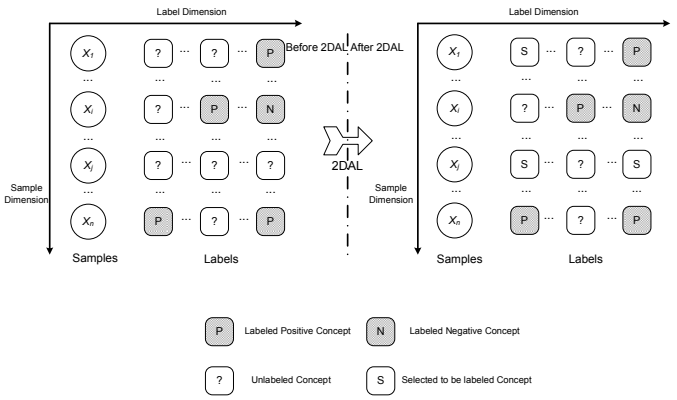

Fig. 1. The proposed two-dimension active learning (2DAL) strategy

well as capture the semantic evolution of the image concept.

II. TWO DIMENSIONAL ACTIVE LEARNING STRATEGY

In this section, we detail the underlying idea of the proposed 2DAL strategy in multi-label setting.

A. Description of 2DAL Framework

Figure 1 illustrates the proposed 2DAL strategy. Different from the typical binary active learning formulation that selects the most informative samples for annotation, we jointly select both the samples and labels simultaneously. The underlying assumption is annotating a portion of well-selected labels provides sufficient information for learning the classifier. As shown in Figure 1, this strategy trades off between the annotation labor and the learning performance along two dimensions, i.e., the sample and label dimensions. In contrast, traditional active learning algorithms can be seen as a one-dimension active selection approach along only sample dimension. More specifically, along label dimension all of the labels correlatively interact. Therefore, once labels are partially annotated, the remaining unlabeled concepts can be inferred based on label correlations. Theoretically, the label correlations have a connection with the expected Bayesian Error Bound (see the following lemma and theorem in section II-B), and thus these label correlations can help to reduce the prediction errors in the testing set during the active learning procedure. This approach saves much labor compared to fully annotating multiple labels especially when the number of labels is huge.

It is worth noting that as illustrated in Figure 1, during 2DAL process, samples may have incomplete labels since the set is only partially labeled. This is different from traditional active learning algorithm. In the Section IV-B, we will address how to learn the classification model from incomplete labels.

B. Multi-label Bayesian error bound

2DAL learner requests annotations on the basis of sample-label pairs which, once incorporated into the training set, are expected to result in the lowest classification error. Here we will first derive a *multi-label Bayesian Error Bound* when a sample-label pair is selected under multi-label setting. 2DAL will iteratively select the ones to minimize this bound.

We begin by defining some notations. For each sample $\boldsymbol{x}$, it has m labels $y_i (1 \leq i \leq m)$ each of which indicates whether its corresponding concept occurs. As stated before, in each 2DAL iteration, some of these labels have already been annotated while others not. Let $U(\boldsymbol{x}) \triangleq \{i|(\boldsymbol{x}, y_i)$ is unlabeled sample-label pair.$\}$ denote the set of indices of unlabeled part and $L(\boldsymbol{x}) \triangleq \{i|(\boldsymbol{x}, y_i)$ is labeled sample-label pair.$\}$ denote the labeled part for $\boldsymbol{x}$. Note that $L(\boldsymbol{x})$ can be an empty set $\varnothing$, which indicates that no label has been annotated for $\boldsymbol{x}$. Let $P(\boldsymbol{y}|\boldsymbol{x})$ be the conditional distribution over samples, where $\boldsymbol{y} = \{0,1\}^m$ is the complete label vector and $P(\boldsymbol{x})$ be the sample distribution.

First, we establish a Bayesian error bound for classifying one unlabeled y_i once y_s is selected for annotating. This error bound originates from the equivocation bound given in [15], and we extend it to multi-label setting so it can handle sample-label pairs.

Lemma 1: Consider a sample $\mathbf{x}$ and its index set of labeled part $U(\mathbf{x})$ and unlabeled part $L(\mathbf{x})$. Once an unlabeled y_s is selected to request annotation (but not yet know its label), the Bayesian classification error $\mathcal{E}\left(y_i|y_s, y_{L(\mathbf{x})}, \mathbf{x}\right)$ for an unlabeled $y_i, i \in U(\mathbf{x})$ is bounded as

$$\begin{aligned} &\tfrac{1}{2}H\left(y_i|y_s; y_{L(\mathbf{x})}, \mathbf{x}\right) - \epsilon \leq \mathcal{E}\left(y_i|y_s; y_{L(\mathbf{x})}, \mathbf{x}\right) \\ &\leq \tfrac{1}{2}H\left(y_i|y_s; y_{L(\mathbf{x})}, \mathbf{x}\right) \end{aligned} \tag{1}$$

where

$$\begin{aligned} &H\left(y_i|y_s; y_{L(\mathbf{x})}, \mathbf{x}\right) = \sum_{t,r\in\{0,1\}}\{-P\left(y_i = t, y_s = r|y_{L(\mathbf{x})}, \mathbf{x}\right) \\ &\times \log P\left(y_i = t|y_s = r; y_{L(\mathbf{x})}, \mathbf{x}\right)\} \end{aligned}$$

is the conditional entropy of y_i given the selected part y_s (both y_i and y_s are random variables because they have not been labeled) and the known labeled part $y_{L(\mathbf{x})}$; $\epsilon = \frac{1}{2}\log\frac{5}{4}$ is a constant.

This lemma will be proven in the appendix I.

Remark 1: It is worthy of noting that this bound is irrelevant to the true label of the selected y_s. In fact, before the annotator gives the label of y_s, the true value of y_s is unknown. However, no matter what y_s holds, 1 or 0, this bound always holds.

Based on this lemma, we can obtain the following theorem which bounds the multi-label error:

Theorem 1: (Multi-label Bayesian classification error bound) Under the condition of lemma 1, the Bayesian classification error bound $\mathcal{E}(\boldsymbol{y}|y_s; y_{L(\boldsymbol{x})}, \boldsymbol{x})$ for sample $\boldsymbol{x}$ is

$$\begin{aligned} &\mathcal{E}\left(\boldsymbol{y}|y_s; y_{L(\boldsymbol{x})}, \boldsymbol{x}\right) \triangleq \tfrac{1}{m}\sum_{i=1}^{m}\mathcal{E}\left(y_i|y_s; y_{L(\boldsymbol{x})}, \boldsymbol{x}\right) \\ &\leq \tfrac{1}{2m}\sum_{i=1}^{m}\left\{H\left(y_i|y_{L(\boldsymbol{x})}, \boldsymbol{x}\right) - MI\left(y_i; y_s|y_{L(\boldsymbol{x})}, \boldsymbol{x}\right)\right\} \end{aligned} \tag{2}$$

where $MI(y_i; y_s|y_{L(\boldsymbol{x})}, \boldsymbol{x})$ is the mutual information between the random variables y_i and y_s given the known labeled part $y_{L(\boldsymbol{x})}$.

Proof:

$$\begin{aligned}&\mathcal{E}\left(\boldsymbol{y}|y_s;y_{L(\boldsymbol{x})},\boldsymbol{x}\right)\\&\overset{(1)}{=}\tfrac{1}{m}\textstyle\sum_{i=1}^{m}\mathcal{E}\left(y_i|y_s;y_{L(\boldsymbol{x})},\boldsymbol{x}\right)\\&\overset{(2)}{\leq}\tfrac{1}{2m}\textstyle\sum_{i=1}^{m}H\left(y_i|y_s;y_{L(\boldsymbol{x})},\boldsymbol{x}\right)\\&\overset{(3)}{=}\tfrac{1}{2m}\textstyle\sum_{i=1}^{m}\left\{H\left(y_i|y_{L(\boldsymbol{x})},\boldsymbol{x}\right)-MI\left(y_i;y_s|y_{L(\boldsymbol{x})},\boldsymbol{x}\right)\right\}\end{aligned}\tag{3}$$

where (1) is the definition of multi-label classification error, (2) directly follows Lemma 1, and (3) makes use of the relationship between mutual information and entropy: $MI(X;Y)=H(X)-H(X|Y)$. ■

With the above theorem, we will derive the 2DAL selection strategy in the following subsection.

C. Pool-base Two-Dimensional Multi-Label Active Learning

We are concerned with *pool-based active learning*, i.e., a large pool $\mathcal{P}$ is available to the learner sampled from $P(\boldsymbol{x})$ and then the proposed 2DAL elaborately selects the sample-label pairs from this pool to reduce the expected classification error. We first write the expected Bayesian classification error over all samples in $\mathcal{P}$ before selecting a sample-label pair $(\boldsymbol{x}_s,y_s)$

$$\mathcal{E}^b\left(\mathcal{P}\right)=\frac{1}{|\mathcal{P}|}\sum\nolimits_{\boldsymbol{x}\in\mathcal{P}}\mathcal{E}\left(\boldsymbol{y}|y_{L(\boldsymbol{x})},\boldsymbol{x}\right)\tag{4}$$

We can use the above classification error on the pool to estimate the expected error over the full distribution $P(\boldsymbol{x})$, i.e., $E_{P(\boldsymbol{x})}\mathcal{E}\left(\boldsymbol{y}|y_{L(\boldsymbol{x})},\boldsymbol{x}\right)=\int P(\boldsymbol{x})\mathcal{E}\left(\boldsymbol{y}|y_{L(\boldsymbol{x})},\boldsymbol{x}\right)d\boldsymbol{x}$, because the pool not only provides a finite set of samples but also an estimation of $P(\boldsymbol{x})$. After selecting the pair $(\boldsymbol{x}_s,y_s)$, the expected Bayesian classification error over the pool $\mathcal{P}$ is

$$\begin{aligned}&\mathcal{E}^a\left(\mathcal{P}\right)\\&=\tfrac{1}{|\mathcal{P}|}\left\{\mathcal{E}\left(\boldsymbol{y}|y_s;y_{L(\boldsymbol{x}_s)},\boldsymbol{x}_s\right)+\textstyle\sum_{\boldsymbol{x}\in\mathcal{P}\setminus\boldsymbol{x}_s}\mathcal{E}\left(\boldsymbol{y}|y_{L(\boldsymbol{x})},\boldsymbol{x}\right)\right\}\\&=\tfrac{1}{|\mathcal{P}|}\{\mathcal{E}\left(\boldsymbol{y}|y_s;y_{L(\boldsymbol{x}_s)},\boldsymbol{x}_s\right)-\mathcal{E}\left(\boldsymbol{y}|y_{L(\boldsymbol{x}_s)},\boldsymbol{x}_s\right)\\&+\textstyle\sum_{x\in\mathcal{P}}\mathcal{E}\left(\boldsymbol{y}|y_{L(\boldsymbol{x})},\boldsymbol{x}\right)\}\end{aligned}\tag{5}$$

Therefore, the reduction of the expected Bayesian classification after selecting $(\boldsymbol{x}_s,y_s)$ over the whole pool $\mathcal{P}$ is

$$\Delta\mathcal{E}\left(\mathcal{P}\right)=\mathcal{E}^b\left(\mathcal{P}\right)-\mathcal{E}^a\left(\mathcal{P}\right)\tag{6}$$

Our goal is to select $(\boldsymbol{x}_s^\star,y_s^\star)$ to maximize the above expected error reduction. That is,

$$\begin{aligned}&(\boldsymbol{x}_s^\star,y_s^\star)=\arg\max\nolimits_{\boldsymbol{x}_s\in\mathcal{P},y_s\in U(\boldsymbol{x}_s)}\Delta\mathcal{E}\left(\mathcal{P}\right)\\&=\arg\min\nolimits_{\boldsymbol{x}_s\in\mathcal{P},y_s\in U(\boldsymbol{x}_s)}-\Delta\mathcal{E}\left(\mathcal{P}\right)\end{aligned}\tag{7}$$

Applying Lemma 1 and Theorem 1, we have

$$\begin{aligned}&-\Delta\mathcal{E}\left(\mathcal{P}\right)=\mathcal{E}^a\left(\mathcal{P}\right)-\mathcal{E}^b\left(\mathcal{P}\right)\\&\overset{(1)}{=}\tfrac{1}{|\mathcal{P}|}\{\mathcal{E}\left(\boldsymbol{y}|y_s;y_{L(\boldsymbol{x}_s)},\boldsymbol{x}_s\right)-\mathcal{E}\left(\boldsymbol{y}|y_{L(\boldsymbol{x}_s)},\boldsymbol{x}_s\right)\\&+\textstyle\sum_{\boldsymbol{x}\in\mathcal{P}}\mathcal{E}\left(\boldsymbol{y}|y_{L(\boldsymbol{x})},\boldsymbol{x}\right)\}-\tfrac{1}{|\mathcal{P}|}\textstyle\sum_{\boldsymbol{x}\in\mathcal{P}}\mathcal{E}\left(\boldsymbol{y}|y_{L(\boldsymbol{x})},\boldsymbol{x}\right)\\&=\tfrac{1}{|\mathcal{P}|}\left\{\mathcal{E}\left(\boldsymbol{y}|y_s;y_{L(\boldsymbol{x}_s)},\boldsymbol{x}_s\right)-\mathcal{E}\left(\boldsymbol{y}|y_{L(\boldsymbol{x}_s)},\boldsymbol{x}_s\right)\right\}\\&\overset{(2)}{\leq}\tfrac{1}{|\mathcal{P}|}\{\tfrac{1}{2m}\textstyle\sum_{i=1}^{m}H\left(y_i|y_{L(\boldsymbol{x}_s)},\boldsymbol{x}_s\right)\\&-\tfrac{1}{2m}\textstyle\sum_{i=1}^{m}MI\left(y_i;y_s|y_{L(\boldsymbol{x}_s)},\boldsymbol{x}_s\right)\\&-\tfrac{1}{m}\textstyle\sum_{i=1}^{m}\mathcal{E}\left(y_i|y_{L(\boldsymbol{x}_s)},\boldsymbol{x}_s\right)\}\\&\overset{(3)}{\leq}\tfrac{1}{|\mathcal{P}|}\{\tfrac{1}{2m}\textstyle\sum_{i=1}^{m}H\left(y_i|y_{L(\boldsymbol{x}_s)},\boldsymbol{x}_s\right)\\&-\tfrac{1}{2m}\textstyle\sum_{i=1}^{m}MI\left(y_i;y_s|y_{L(\boldsymbol{x}_s)},\boldsymbol{x}_s\right)\\&-\tfrac{1}{m}\textstyle\sum_{i=1}^{m}\left(\tfrac{1}{2}H\left(y_i|y_{L(\boldsymbol{x}_s)},\boldsymbol{x}_s\right)-\epsilon\right)\}\\&=\tfrac{1}{|\mathcal{P}|}\left\{\epsilon-\tfrac{1}{2m}\textstyle\sum_{i=1}^{m}MI\left(y_i;y_s|y_{L(\boldsymbol{x}_s)},\boldsymbol{x}_s\right)\right\}\end{aligned}\tag{8}$$

The equality (1) comes from Eqn. (4) (5). The first inequality (2) follows the Theorem 1 and the second inequality (3) comes from the lower bound of Lemma 1.

Consequently, by minimizing the obtained Bayesian error bound (8), we can select the sample-label pair for annotation as

$$\begin{aligned}&(\boldsymbol{x}_s^\star,y_s^\star)\\&=\underset{\boldsymbol{x}_s\in\mathcal{P},y_s\in U(\boldsymbol{x}_s)}{\arg\min}\tfrac{1}{|\mathcal{P}|}\left\{\epsilon-\tfrac{1}{2m}\sum_{i=1}^{m}MI\left(y_i;y_s|y_{L(\boldsymbol{x}_s)},\boldsymbol{x}_s\right)\right\}\\&=\underset{\boldsymbol{x}_s\in\mathcal{P},y_s\in U(\boldsymbol{x}_s)}{\arg\max}\textstyle\sum_{i=1}^{m}MI\left(y_i;y_s|y_{L(\boldsymbol{x}_s)},\boldsymbol{x}_s\right)\end{aligned}\tag{9}$$

D. Further Discussions

1 As discussed in section II-A, the proposed 2DAL approach is an active learning algorithm along two dimensions, which reduces not only *sample uncertainty* but also *label uncertainty*. The above selection strategy Eqn. (9) well reflects these two targets. The last term in Eqn. (9) can be rewritten as

$$\begin{aligned}&\textstyle\sum_{i=1}^{m}MI\left(y_i;y_s|y_{L(\boldsymbol{x}_s)},\boldsymbol{x}_s\right)\\&=MI\left(y_s;y_s|y_{L(\boldsymbol{x}_s)},\boldsymbol{x}_s\right)+\sum_{i=1,i\neq s}^{m}MI\left(y_i;y_s|y_{L(\boldsymbol{x}_s)},\boldsymbol{x}_s\right)\\&=H\left(y_s|y_{L(\boldsymbol{x}_s)},\boldsymbol{x}_s\right)+\sum_{i=1,i\neq s}^{m}MI\left(y_i;y_s|y_{L(\boldsymbol{x}_s)},\boldsymbol{x}_s\right)\end{aligned}\tag{10}$$

As we can see, the objective selection function for 2DAL has been divided into two parts: $H\left(y_s|y_{L(\boldsymbol{x}_s)},\boldsymbol{x}_s\right)$ and $\sum_{i=1,i\neq s}^{m}MI\left(y_i;y_s|y_{L(\boldsymbol{x}_s)},\boldsymbol{x}_s\right)$. The former entropy measures the uncertainty of the selected pair $(\boldsymbol{x}_s^\star,y_s^\star)$ itself, which is consistent with the typical one dimensional active learning algorithm, i.e., to select the most "informative" (uncertain) samples near the classification boundary [16] [2] [17]. On the other hand, the latter mutual information terms measure the statistical redundancy among the selected label and the rest ones. By maximizing these mutual information terms, 2DAL provides maximum information to reduce the uncertainty of the other labels. This

2DAL strategy complies with our motivation of selecting sample-label pairs reducing the uncertainties along both *sample* and *label* dimensions. Note that when there is only one label associated with each sample, the selection criterion of Eqn. (10) reduces to $H(y_s|\boldsymbol{x}_s)$ which is the same as the traditional binary-based criterion, i.e., to select the most uncertain sample for annotation [17] [9]. Thus the traditional binary-based active learning can be seen as a special case of the 2DAL strategy with a single label.

2 It is worthy of indicating that the posterior $P(\boldsymbol{y}|\boldsymbol{x})$ needs to capture the label correlations in the proposed 2DAL strategy. If we assume the independence among the different labels, i.e., $P(\boldsymbol{y}|\boldsymbol{x}) = \prod_{i=1}^{m} P(y_i|\boldsymbol{x})$, the corresponding mutual information terms will become $MI\left(y_i; y_s|y_{L(\boldsymbol{x}_s)}, \boldsymbol{x}_s\right) = 0, i \neq s$. In this case, the selection criterion reduces to $(\boldsymbol{x}_s^\star, y_s^\star) = \arg\max_{\boldsymbol{x}_s \in \mathcal{P}, y_s \in U(\boldsymbol{x}_s)} H\left(y_s|y_{L(\boldsymbol{x}_s)}, \boldsymbol{x}_s\right)$, i.e., to select the most uncertain sample-label pair. Such a criterion neglects the label correlations and would become less efficient to reduce label uncertainty. Therefore, a statistical method that models the label correlations is required in this case. We will develop an efficient Bayesian model in the following section.

3 When computing the mutual information terms in Eqn. (9), we need the distribution $P(\boldsymbol{y}|\boldsymbol{x})$. However, the true distribution is unknown, but we can estimate it using the current learner. As stated in [18], such an approximation is reasonable because the most useful labeling is usually consistent with the learner's prior belief over the majority (but not all) of the unlabeled pairs.

III. MULTI-LABEL ONLINE LEARNER

Once new sample-label pairs are selected according to the 2DAL strategy, the statistical model for multi-label images should be updated accordingly. However, as stated in Section I, the conventional offline algorithms retrain a new model on the whole historically-collected training set plus the new samples. It will become intractable when hundreds of thousands of samples are accumulated into the training set over time. Therefore, an efficient online adaptation algorithm is desired to adapt the old model to the new sample without retraining it. Intuitively, such an online classification algorithm should satisfy the following requirements:

- It ought to preserve the old knowledge that has already existed in the old model. This knowledge stores the rich historical information about the previously-acquired training samples;
- It can reveal the information contained in the newly-arrived multi-label samples. In contrast to the traditional binary-based algorithm (e.g., one-against-rest SVM), the label correlations must be modeled in this online learner.

In this section, we will present such an online learning algorithm that satisfies the above two requirements. We begin our discussion with the definition of some notations and the online setting. Under the online setting, we are given an existing old multi-label model $P^\tau(\boldsymbol{y}|\boldsymbol{x})$, which is trained from the historically-acquired images. Then a set of new images and their corresponding labels $\{\boldsymbol{x}_i, \boldsymbol{y}_i\}_{i=1}^n$ is obtained in each 2DAL iteration. Each $\boldsymbol{x}_i \in \mathbb{R}^d$ is the feature vector and $\boldsymbol{y}_i \in \{0,1\}^m$ is a m-dimensional label vector, in which m is the number of image labels and each element in $\boldsymbol{y}_i$ indicates the membership for the corresponding label. Our goal is to learn a new model $P^{\tau+1}(\boldsymbol{y}|\boldsymbol{x})$ based on the existing model $P^\tau(\boldsymbol{y}|\boldsymbol{x})$ and $\{\boldsymbol{x}_i, \boldsymbol{y}_i\}_{i=1}^n$. In contrast to the retraining-based learning algorithm, the online learner does not utilize the historical training set but only the current new coming samples. It assumes the information about the historical training samples has been preserved in the old model $P^\tau(\boldsymbol{y}|\boldsymbol{x})$, which is learned from these old samples. Thus with much fewer of only new coming samples, the online learner can train a new model efficiently.

As aforementioned, this new model $P^{\tau+1}(\boldsymbol{y}|\boldsymbol{x})$ ought to satisfy the two requirements: preserving the existing knowledge in $P^\tau(\boldsymbol{y}|\boldsymbol{x})$ while revealing the information in new samples $\{\boldsymbol{x}_i, \boldsymbol{y}_i\}_{i=1}^n$. These two requirements can be satisfied by formulating the following probabilistic variational problem. In this paper, we use the Kullback-Leibler Divergence (KLD) [19] to measure the degree of the new model preserving the existing knowledge contained in the old one, under a set of multi-label constraints revealing the information contained in the new samples:

$$\widehat{P}^{\tau+1}(\boldsymbol{y}|\boldsymbol{x}) = \arg\min_{P^{\tau+1}} \left\langle D_{KL}\left(P^{\tau+1}(\boldsymbol{y}|\boldsymbol{x})||P^\tau(\boldsymbol{y}|\boldsymbol{x})\right)\right\rangle_{\widetilde{P}(\boldsymbol{x})} \quad (11)$$

$$s.t.\ \langle y_i\rangle_{P^{\tau+1}(\boldsymbol{x},\boldsymbol{y})} = \langle y_i\rangle_{\widetilde{P}(\boldsymbol{x},\boldsymbol{y})} + \eta_i, 1 \leq i \leq m \quad (12)$$

$$\langle y_i y_j\rangle_{P^{\tau+1}(\boldsymbol{x},\boldsymbol{y})} = \langle y_i y_j\rangle_{\widetilde{P}(\boldsymbol{x},\boldsymbol{y})} + \theta_{ij}, 1 \leq i < j \leq m \quad (13)$$

$$\langle y_i x_l\rangle_{P^{\tau+1}(\boldsymbol{x},\boldsymbol{y})} = \langle y_i x_l\rangle_{\widetilde{P}(\boldsymbol{x},\boldsymbol{y})} + \phi_{il}, 1 \leq i \leq m, 1 \leq l \leq d \quad (14)$$

$$\sum\nolimits_{\boldsymbol{y}} P^{\tau+1}(\boldsymbol{y}|\boldsymbol{x}) = 1 \quad (15)$$

where $\left\langle D_{KL}\left(P^{\tau+1}(\boldsymbol{y}|\boldsymbol{x})||P^\tau(\boldsymbol{y}|\boldsymbol{x})\right)\right\rangle_{\widetilde{P}(\boldsymbol{x})}$ is the KLD between the new model $P^{\tau+1}(\boldsymbol{y}|\boldsymbol{x})$ and the old one $P^\tau(\boldsymbol{y}|\boldsymbol{x})$ over the sample frequency $\widetilde{P}(\boldsymbol{x}) = \frac{1}{m}\sum_{i=1}^m \delta(\boldsymbol{x} - \boldsymbol{x}_i)$ taken from $\{\boldsymbol{x}_i\}_{i=1}^n$ where $\delta(\cdot)$ is the indicator function. Thus we have

$$\begin{aligned}
&\left\langle D_{KL}\left(P^{\tau+1}(\boldsymbol{y}|\boldsymbol{x})||P^\tau(\boldsymbol{y}|\boldsymbol{x})\right)\right\rangle_{\widetilde{P}(\boldsymbol{x})} \\
&= \sum\nolimits_{\boldsymbol{x}} \widetilde{P}(\boldsymbol{x}) D_{KL}\left(P^{\tau+1}(\boldsymbol{y}|\boldsymbol{x})||P^\tau(\boldsymbol{y}|\boldsymbol{x})\right) \\
&= \sum_{i=1}^{n} D_{KL}\left(P^{\tau+1}(\boldsymbol{y}|\boldsymbol{x}_i)||P^\tau(\boldsymbol{y}|\boldsymbol{x}_i)\right)
\end{aligned} \quad (16)$$

$\langle\cdot\rangle_{P^{\tau+1}(\boldsymbol{x},\boldsymbol{y})}$ and $\langle\cdot\rangle_{\widetilde{P}(\boldsymbol{x},\boldsymbol{y})}$ in Eqn. (12) $\sim$ (14) denote the expectation w.r.t. model distribution $P^{\tau+1}(\boldsymbol{x},\boldsymbol{y})$ and empirical distribution $\widetilde{P}(\boldsymbol{x},\boldsymbol{y}) = \frac{1}{m}\sum_{i=1}^m \delta(\boldsymbol{x} - \boldsymbol{x}_i)\cdot\delta(\boldsymbol{y} - \boldsymbol{y}_i)$ on the training samples $\{\boldsymbol{x}_i, \boldsymbol{y}_i\}_{i=1}^n$, respectively. y_i, y_j and x_l in these $\langle\cdot\rangle$ represent the ith and jth elements in label vectors $\boldsymbol{y}$ and lth element in feature vectors $\boldsymbol{x}$, respectively. It is worth noting that the joint model distribution $P^{\tau+1}(\boldsymbol{x},\boldsymbol{y}) = P^{\tau+1}(\boldsymbol{y}|\boldsymbol{x})\widetilde{P}(\boldsymbol{x})$, i.e., we only care about the conditional distribution $P^{\tau+1}(\boldsymbol{y}|\boldsymbol{x})$ and thus use the sample frequency $\widetilde{P}(\boldsymbol{x})$ on the training samples to approximate the true sample distribution $P^{\tau+1}(\boldsymbol{x})$. Constraints (12) $\sim$ (14)

restrict the new model to comply with the statistics on the new samples. It is similar to the conventional offline model used in the previous work [20] [4]. $\eta_i \sim N(0, \sigma_\eta^2)$, $\theta_{ij} \sim N(0, \sigma_\theta^2)$ and $\phi_{il} \sim N(0, \sigma_\phi^2)$ are the estimation errors following the Gaussian distribution which serve to smooth $P^{\tau+1}(\boldsymbol{y}|\boldsymbol{x})$ to improve the model's generalization ability. These estimation error distributions can be due to the noise in the training samples. Note that we do not assume any specific probabilistic form of $P^{\tau+1}(\boldsymbol{y}|\boldsymbol{x})$ and $P^{\tau}(\boldsymbol{y}|\boldsymbol{x})$. Therefore, the objective function is minimized by exploring all possible input functions instead of some parameterized functions like in the conventional optimization problem. This type of optimization objective is called variational optimization (see more detail about variational optimization in [21]). With no assumption of any specific probabilistic form, the variational optimization problem can search in a much larger functional space to find a more optimal one.

The above objective function (16) has a rather intuitive explanation. From the perspective of the information theory [19], the KLD measures the distance between two different distributions. Thus by minimizing the KLD between $P^{\tau+1}(\boldsymbol{y}|\boldsymbol{x})$ and $P^{\tau}(\boldsymbol{y}|\boldsymbol{x})$, the new model $P^{\tau+1}(\boldsymbol{y}|\boldsymbol{x})$ can preserve the old knowledge in the existing model $P^{\tau}(\boldsymbol{y}|\boldsymbol{x})$ as much as possible. This is consistent with the first requirement above. On the other hand, in the multi-label constraints (12) (13) (14), we force the new model $P^{\tau+1}(\boldsymbol{y}|\boldsymbol{x})$ to comply with three statistics on the new samples $\{\boldsymbol{x}_i, \boldsymbol{y}_i\}_{i=1}^n$. It satisfies the second requirement that the new model must comply with the information contained in the new samples. It is worth noting that by modeling the label correlations in Eqn. (13), the obtained model reveals the underlying correlations between different labels. Finally, the constraint (15) just serves to normalize $P^{\tau+1}(\boldsymbol{y}|\boldsymbol{x})$. Figure 2 illustrates the geometry explanation of this online learner. Here $\mathcal{D}$ denotes a space in which each point is a potential conditional distributions $P(\boldsymbol{y}|\boldsymbol{x})$ for the new model. This space is equipped with KLD as its distance metric. All the distributions satisfying the multi-label constraints constitute a sub-manifold $\mathcal{H}$ embedded in $\mathcal{D}$. Therefore, the above optimization problem equals to find an optimal new model $P^{\tau+1}(\boldsymbol{y}|\boldsymbol{x})$ in $\mathcal{H}$ with the minimum distance from the old model $P^{\tau}(\boldsymbol{y}|\boldsymbol{x})$. Equivalently, from the Geometrical prospective, the optimal solution $P^{\tau+1}(\boldsymbol{y}|\boldsymbol{x})$ to this problem is a projection of the old model $P^{\tau}(\boldsymbol{y}|\boldsymbol{x})$ to the sub-manifold $\mathcal{H}$.

As stated in Section I, when learning the new model we should balance between the existing knowledge and the new information. The Gaussian error estimations in (12) (13) (14) serve to provide such a trading-off scheme. When the variances of Gaussian errors η_i, θ_{ij} and ϕ_{il} are larger, the new model $P^{\tau+1}(\boldsymbol{y}|\boldsymbol{x})$ will be biased to be the existing model $P^{\tau}(\boldsymbol{y}|\boldsymbol{x})$ since the multi-label constraints become more relaxed with relatively large noises η_i, θ_{ij} and ϕ_{il} in the current training set. In contrast, the small variances will make $P^{\tau+1}(\boldsymbol{y}|\boldsymbol{x})$ bias on the new information in $\{\boldsymbol{x}_i, \boldsymbol{y}_i\}_{i=1}^n$. Extremely, the removal of these error estimations will lead to a new model that completely comply with the new information. Furthermore, as to been derived later, these Gaussian errors will introduce a regularizer term in the dual form of this formulation. As suggested in [22] [4], they assume the joint probability of estimation errors should

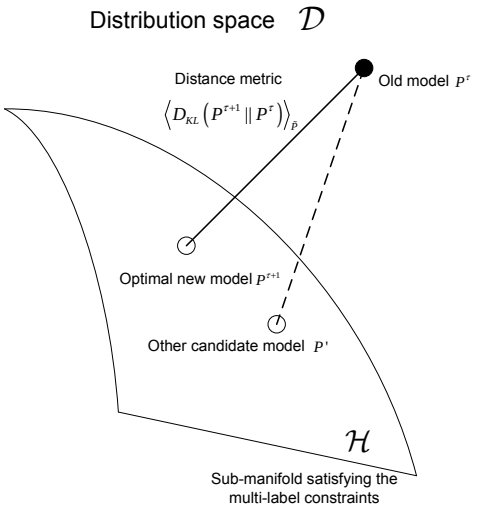

Fig. 2. A Geometry explanation of the proposed online learner. $\mathcal{D}$ is a space of all potential distributions for the new model. It is equipped with KLD as its distance metric. All the distributions satisfying the multi-label constraints constitute a sub-manifold $\mathcal{H}$. The optimal new model $P^{\tau+1}(\boldsymbol{y}|\boldsymbol{x})$ can be seen as the projection of the old model $P^{\tau}(\boldsymbol{y}|\boldsymbol{x})$ to the sub-manifold $\mathcal{H}$. In this figure, $P^{\tau+1}$ is the optimal new model and we can see its distance to the old model is less than that of any other candidate models P' in the sub-manifold $\mathcal{H}$.

be reasonably large, e.g., $P(\eta_i, \theta_{ij}, \phi_{il} | 1 \leq i < j \leq m, 1 \leq l \leq d) \geq \varepsilon$. Substitute $\eta_i \sim N(0, \sigma_\eta^2) = \frac{1}{\sqrt{2\pi}\sigma_\eta} \exp\{-\frac{\eta_i^2}{2\sigma_\eta^2}\}$, $\theta_{ij} \sim N(0, \sigma_\theta^2) = \frac{1}{\sqrt{2\pi}\sigma_\theta} \exp\{-\frac{\theta_{ij}^2}{2\sigma_\theta^2}\}$ and $\phi_{il} \sim N(0, \sigma_\phi^2) = \frac{1}{\sqrt{2\pi}\sigma_\phi} \exp\{-\frac{\phi_{il}^2}{2\sigma_\phi^2}\}$ into this inequality and assume these estimate errors are independent to each other, we have

$$\sum_i \frac{\eta_i^2}{2\sigma_\eta^2 \big/ n} + \sum_{i<j} \frac{\theta_{ij}^2}{2\sigma_\theta^2 \big/ n} + \sum_{i,l} \frac{\phi_{il}^2}{2\sigma_\phi^2 \big/ n} \leq C \qquad (17)$$

Before moving further, we briefly discuss how the above online formulation tackles "concept drift" over time mentioned in section I. There already exist literatures working on this "concept drift" problem [16] [23]. From statistical perspective, "concept drift" can be modeled as the change of empirical distribution of the samples and the labels (i.e., the joint distribution of the samples and the labels) over time [16]. As indicated by Eqn. (12) $\sim$ (14), the proposed online model adapts to the new empirical distribution $\widetilde{P}(\boldsymbol{x}, \boldsymbol{y})$ by complying with the first and second order statistics of $\widetilde{P}(\boldsymbol{x}, \boldsymbol{y})$. Through such a model adaptation, "concept drift" can be automatically captured by this online adaptation model.

Combining the formulations (16) $\sim$ (15) and (17), according to Karush-Kuhn-Tucker (KKT) conditions $P^{\tau+1}(\boldsymbol{y}|\boldsymbol{x})$ can

be solved by maximizing the dual Lagrange function

$$\begin{aligned}
&\mathcal{L}\left(P^{\tau+1}(\boldsymbol{y}|\boldsymbol{x}),\eta,\theta,\phi,\boldsymbol{b},\boldsymbol{R},\boldsymbol{W},\gamma,\varsigma\right)\\
&=\left\langle D_{KL}\left(P^{\tau+1}(\boldsymbol{y}|\boldsymbol{x})||P^{\tau}(\boldsymbol{y}|\boldsymbol{x})\right)\right\rangle_{\widetilde{P}(\boldsymbol{x})}\\
&+\sum_i b_i\left(\langle y_i\rangle_{\widetilde{P}(\boldsymbol{x},\boldsymbol{y})}+\eta_i-\langle y_i\rangle_{P^{\tau+1}(\boldsymbol{x},\boldsymbol{y})}\right)\\
&+\sum_{i<j}R_{ij}\left(\langle y_iy_j\rangle_{\widetilde{P}(\boldsymbol{x},\boldsymbol{y})}+\theta_{ij}-\langle y_iy_j\rangle_{P^{\tau+1}(\boldsymbol{x},\boldsymbol{y})}\right)\\
&+\sum_{i,l}W_{il}\left(\langle y_ix_l\rangle_{\widetilde{P}(\boldsymbol{x},\boldsymbol{y})}+\phi_{il}-\langle y_ix_l\rangle_{P^{\tau+1}(\boldsymbol{x},\boldsymbol{y})}\right)\\
&+\gamma\left(\sum_i\frac{\eta_i^2}{2\sigma_\eta^2/n}+\sum_{i<j}\frac{\theta_{ij}^2}{2\sigma_\theta^2/n}+\sum_{i,l}\frac{\phi_{ij}^2}{2\sigma_\phi^2/n}-C\right)\\
&+\textstyle\sum_x\varsigma(x)\left(1-\sum_y P^{\tau+1}(\boldsymbol{y}|\boldsymbol{x})\right)
\end{aligned}\tag{18}$$

where $\boldsymbol{b},\boldsymbol{R},\boldsymbol{W},\gamma,\varsigma$ are Lagrangian multipliers, in which $\boldsymbol{b}=[b_1,b_2,\cdots,b_m]^T$ is a $m\times 1$ column vector, $\boldsymbol{R}=[R_{ij}]_{m\times m}$ is a strict upper matrix with $R_{ij}=0$ for $i\geq j$, and $\boldsymbol{W}=[W_{ij}]_{m\times d}$ is a $m\times d$ matrix. The above function can be maximized by taking its derivatives and setting them to zero. Specifically, the derivative of KLD w.r.t. $P^{\tau+1}(\boldsymbol{y}|\boldsymbol{x})$ is

$$\begin{aligned}
&\frac{\partial\left\langle D_{KL}\left(P^{\tau+1}(\boldsymbol{y}|\boldsymbol{x})||P^{\tau}(\boldsymbol{y}|\boldsymbol{x})\right)\right\rangle_{\widetilde{P}(\boldsymbol{x})}}{\partial P^{\tau+1}(\boldsymbol{y}|\boldsymbol{x})}\\
&=\frac{\partial}{\partial P^{\tau+1}(\boldsymbol{y}|\boldsymbol{x})}\textstyle\sum_\nu\widetilde{P}(\nu)\sum_h P^{\tau+1}(h|\nu)\log\frac{P^{\tau+1}(h|\nu)}{P^{\tau}(h|\nu)}\\
&=\frac{\partial}{\partial P^{\tau+1}(\boldsymbol{y}|\boldsymbol{x})}\textstyle\sum_\nu\widetilde{P}(\nu)\sum_h P^{\tau+1}(h|\nu)\log P^{\tau+1}(h|\nu)\\
&-\frac{\partial}{\partial P^{\tau+1}(\boldsymbol{y}|\boldsymbol{x})}\textstyle\sum_\nu\widetilde{P}(\nu)\sum_h P^{\tau+1}(h|\nu)\log P^{\tau}(h|\nu)\\
&=\widetilde{P}(\boldsymbol{x})\left\{\log P^{\tau+1}(\boldsymbol{y}|\boldsymbol{x})+1-\log P^{\tau}(\boldsymbol{y}|\boldsymbol{x})\right\}
\end{aligned}\tag{19}$$

Thus the derivative of $\mathcal{L}\left(P^{\tau+1}(\boldsymbol{y}|\boldsymbol{x}),\eta,\theta,\phi,\boldsymbol{b},\boldsymbol{R},\boldsymbol{W},\gamma,\varsigma\right)$ w.r.t. $P^{\tau+1}(\boldsymbol{y}|\boldsymbol{x})$ is

$$\begin{aligned}
&\frac{\partial\mathcal{L}}{\partial P^{\tau+1}(\boldsymbol{y}|\boldsymbol{x})}\\
&=\widetilde{P}(\boldsymbol{x})\{\log P^{\tau+1}(\boldsymbol{y}|\boldsymbol{x})+1-\log P^{\tau}(\boldsymbol{y}|\boldsymbol{x})\\
&-\boldsymbol{y}^T(\boldsymbol{b}+\boldsymbol{R}\boldsymbol{y}+\boldsymbol{W}\boldsymbol{x})\}-\varsigma(\boldsymbol{x})
\end{aligned}\tag{20}$$

It is easy to compute the derivatives of Lagrange w.r.t. other parameters η_i, θ_{ij} and ϕ_{il}:

$$\frac{\partial\mathcal{L}}{\partial\eta_i}=b_i+n\gamma\frac{\eta_i}{\sigma_\eta^2};\frac{\partial\mathcal{L}}{\partial\theta_{ij}}=R_{ij}+n\gamma\frac{\theta_{ij}}{\sigma_\theta^2};\frac{\partial\mathcal{L}}{\partial\phi_{il}}=W_{il}+n\gamma\frac{\phi_{il}}{\sigma_\phi^2}.\tag{21}$$

Setting the above derivatives (20) $\sim$ (21) of Lagrange to be zero, we can find when γ is zero, $\boldsymbol{b}$, $\boldsymbol{R}$ and $\boldsymbol{W}$ are also reduced to be the trivial solution zero. Thus we can assume $\gamma>0$, and we obtain

$$P^{\tau+1}(\boldsymbol{y}|\boldsymbol{x})\propto P^{\tau}(\boldsymbol{y}|\boldsymbol{x})\exp\left\{\boldsymbol{y}^T(\boldsymbol{b}+\boldsymbol{R}\boldsymbol{y}+\boldsymbol{W}\boldsymbol{x})\right\}\tag{22}$$

Considering the normalization condition (15), we can get

$$P^{\tau+1}(\boldsymbol{y}|\boldsymbol{x})=\frac{1}{Z^{\tau+1}(\boldsymbol{x})}P^{\tau}(\boldsymbol{y}|\boldsymbol{x})\exp\left\{\boldsymbol{y}^T(\boldsymbol{b}+\boldsymbol{R}\boldsymbol{y}+\boldsymbol{W}\boldsymbol{x})\right\}\tag{23}$$

$$\eta_i=-\frac{\sigma_\eta^2}{n\gamma}b_i,\theta_{ij}=-\frac{\sigma_\theta^2}{n\gamma}R_{ij},\phi_{il}=-\frac{\sigma_\phi^2}{n\gamma}W_{il}\tag{24}$$

where

$$Z^{\tau+1}(\boldsymbol{x})=\textstyle\sum_{\boldsymbol{y}}P^{\tau}(\boldsymbol{y}|\boldsymbol{x})\exp\left\{\boldsymbol{y}^T(\boldsymbol{b}+\boldsymbol{R}\boldsymbol{y}+\boldsymbol{W}\boldsymbol{x})\right\}\tag{25}$$

is the partition function. Now, let us recompute the KLD between $P^{\tau+1}(\boldsymbol{y}|\boldsymbol{x})$ and $P^{\tau}(\boldsymbol{y}|\boldsymbol{x})$ in Eqn. (16) considering (23)

$$\begin{aligned}
&\left\langle D_{KL}\left(P^{\tau+1}(\boldsymbol{y}|\boldsymbol{x})||P^{\tau}(\boldsymbol{y}|\boldsymbol{x})\right)\right\rangle_{\widetilde{P}(\boldsymbol{x})}\\
&=\sum_{\boldsymbol{x},\boldsymbol{y}}\widetilde{P}(\boldsymbol{x})P^{\tau+1}(\boldsymbol{y}|\boldsymbol{x})\log\frac{P^{\tau+1}(\boldsymbol{y}|\boldsymbol{x})}{P^{\tau}(\boldsymbol{y}|\boldsymbol{x})}\\
&=\sum_{\boldsymbol{x},\boldsymbol{y}}\widetilde{P}(\boldsymbol{x})P^{\tau+1}(\boldsymbol{y}|\boldsymbol{x})\log\frac{\exp\left\{\boldsymbol{y}^T(\boldsymbol{b}+\boldsymbol{R}\boldsymbol{y}+\boldsymbol{W}\boldsymbol{x})\right\}}{Z^{\tau+1}(\boldsymbol{x})}\\
&=\sum_{\boldsymbol{x},\boldsymbol{y}}\widetilde{P}(\boldsymbol{x})P^{\tau+1}(\boldsymbol{y}|\boldsymbol{x})\left\{\boldsymbol{y}^T(\boldsymbol{b}+\boldsymbol{R}\boldsymbol{y}+\boldsymbol{W}\boldsymbol{x})\right\}\\
&-\sum_{\boldsymbol{x}}\widetilde{P}(\boldsymbol{x})\log Z^{\tau+1}(\boldsymbol{x})\\
&=\sum_i b_i\langle y_i\rangle_{P^{\tau+1}(\boldsymbol{x},\boldsymbol{y})}+\sum_{i<j}R_{ij}\langle y_iy_j\rangle_{P^{\tau+1}(\boldsymbol{x},\boldsymbol{y})}\\
&+\sum_{i,l}W_{il}\langle y_ix_l\rangle_{P^{\tau+1}(\boldsymbol{x},\boldsymbol{y})}-\left\langle\log Z^{\tau+1}(\boldsymbol{x})\right\rangle_{\widetilde{P}(\boldsymbol{x})}
\end{aligned}\tag{26}$$

Substitute the above equation and (24) into Eqn. (18), we can obtain the Lagrangian Function and the corresponding dual optimization problem to solve the parameters $\boldsymbol{b}$, $\boldsymbol{R}$, $\boldsymbol{W}$

$$\begin{aligned}
&\boldsymbol{b}^\star,\boldsymbol{R}^\star,\boldsymbol{W}^\star=\arg\max_{\boldsymbol{b},\boldsymbol{R},\boldsymbol{W}}\mathcal{L}\left(\boldsymbol{b},\boldsymbol{R},\boldsymbol{W}\right)\\
&\arg\max_{\boldsymbol{b},\boldsymbol{R},\boldsymbol{W}}\left\langle\boldsymbol{y}^T\left(\boldsymbol{b}+\boldsymbol{R}\boldsymbol{y}+\boldsymbol{W}\boldsymbol{x}\right)-\log Z^{\tau+1}(\boldsymbol{x})\right\rangle_{\widetilde{P}(\boldsymbol{x},\boldsymbol{y})}\\
&-\tfrac{\alpha_b}{2n}||\boldsymbol{b}||_2^2-\tfrac{\alpha_R}{2n}||\boldsymbol{R}||_F^2-\tfrac{\alpha_W}{2n}||\boldsymbol{W}||_F^2\\
&=\arg\max_{\boldsymbol{b},\boldsymbol{R},\boldsymbol{W}}\sum_{i=1}^n\left\{\boldsymbol{y}_i^T\left(\boldsymbol{b}+\boldsymbol{R}\boldsymbol{y}_i+\boldsymbol{W}\boldsymbol{x}_i\right)-\log Z^{\tau+1}(\boldsymbol{x}_i)\right\}\\
&-\tfrac{\alpha_b}{2n}||\boldsymbol{b}||_2^2-\tfrac{\alpha_R}{2n}||\boldsymbol{R}||_F^2-\tfrac{\alpha_W}{2n}||\boldsymbol{W}||_F^2
\end{aligned}\tag{27}$$

with

$$\alpha_{\boldsymbol{b}}=\sigma_\eta^2\big/\gamma,\alpha_{\boldsymbol{R}}=\sigma_\theta^2\big/\gamma,\alpha_{\boldsymbol{W}}=\sigma_\phi^2\big/\gamma.\tag{28}$$

where $||\cdot||_2$ and $||\cdot||_F$ are norm-2 and Frobenius norm respectively. Here, $-\frac{\alpha_b}{2n}||\boldsymbol{b}||_2^2-\frac{\alpha_R}{2n}||\boldsymbol{R}||_F^2-\frac{\alpha_W}{2n}||\boldsymbol{W}||_F^2$ serves as regularization term. Note that in this dual optimization problem, the old model $P^{\tau}(\boldsymbol{y}|\boldsymbol{x})$ affects the objective function through the partition function $Z^{\tau+1}(\boldsymbol{x})$ of Eqn. (25). Moreover, according to the last equality in Eqn. (27) the summation is only taken over the newly-acquired samples, instead of all the historically-accumulated training set like the offline learner. Thus with a rather smaller number of new samples, the above optimization problem can be solved much more efficiently for the proposed online learner.

Take the derivatives of $\mathcal{L}\left(\boldsymbol{b},\boldsymbol{R},\boldsymbol{W}\right)$ w.r.t. $\boldsymbol{b}$, $\boldsymbol{R}$, $\boldsymbol{W}$

$$\begin{aligned}
&\frac{\partial\mathcal{L}}{\partial b_i}=\langle y_i\rangle_{\widetilde{P}(\boldsymbol{x},\boldsymbol{y})}-\langle y_i\rangle_{P^{\tau+1}(\boldsymbol{x},\boldsymbol{y})}-\tfrac{\alpha_b}{n}b_i\\
&\frac{\partial\mathcal{L}}{\partial R_{ij}}=\langle y_iy_j\rangle_{\widetilde{P}(\boldsymbol{x},\boldsymbol{y})}-\langle y_iy\rangle_{P^{\tau+1}(\boldsymbol{x},\boldsymbol{y})}-\tfrac{\alpha_R}{n}R_{ij}\\
&\frac{\partial\mathcal{L}}{\partial W_{il}}=\langle y_ix_l\rangle_{\widetilde{P}(\boldsymbol{x},\boldsymbol{y})}-\langle y_ix_l\rangle_{P^{\tau+1}(\boldsymbol{x},\boldsymbol{y})}-\tfrac{\alpha_W}{n}W_{il}
\end{aligned}\tag{29}$$

Given the above derivatives, we can use the efficient gradient descent methods (such as L-BFGS [24]) to maximize (27).

Here we would like to have a brief discussion about the optimization problem (27). By setting the larger variances $\sigma_\eta^2,\sigma_\eta^2,\sigma_\phi^2$, it says there exists considerable noise in the new samples $\{\boldsymbol{x}_i,\boldsymbol{y}_i\}_{i=1}^n$ (see Eqn. (12), (13), (14)). At this time, according to the regularization term in (27), the smaller parameters $\boldsymbol{b}$, $\boldsymbol{R}$, $\boldsymbol{W}$ are preferred. Thus, the new model $P^{\tau+1}(\boldsymbol{y}|\boldsymbol{x})$ will approach to the old one. Conversely, $P^{\tau+1}(\boldsymbol{y}|\boldsymbol{x})$ will more consider the new samples. So by setting different $\sigma_\eta^2,\sigma_\eta^2,\sigma_\phi^2$, we can make balance between old knowledge in $P^{\tau+1}(\boldsymbol{y}|\boldsymbol{x})$ and new information in $\{\boldsymbol{x}_i,\boldsymbol{y}_i\}_{i=1}^n$. Such a balance is useful when the semantic meaning of

image concept is changing over time, as well as the number of the new training samples is rather smaller than that of historical training samples (See Section I for detail).

Note that when deriving $P^{\tau+1}(\boldsymbol{y}|\boldsymbol{x})$ in Eqn. (23), we do not assume any specific probabilistic form of the old model $P^{\tau}(\boldsymbol{y}|\boldsymbol{x})$. Thus any statistical model can be used as $P^{\tau}(\boldsymbol{y}|\boldsymbol{x})$, such as logistic regression model and Gaussian process model. However without loss of generality, we can assume $P^{\tau}(\boldsymbol{y}|\boldsymbol{x})$ has the following form

$$P^{\tau}(\boldsymbol{y}|\boldsymbol{x}) = \frac{1}{Z^{\tau}(\boldsymbol{x})} \exp\left\{\boldsymbol{y}^T(\boldsymbol{b}^{\tau} + \boldsymbol{R}^{\tau}\boldsymbol{y} + \boldsymbol{W}^{\tau}\boldsymbol{x})\right\} \tag{30}$$

where $Z^{\tau}(\boldsymbol{x}) = \sum_{\boldsymbol{y}} \exp\left\{\boldsymbol{y}^T(\boldsymbol{b}^{\tau} + \boldsymbol{R}^{\tau}\boldsymbol{y} + \boldsymbol{W}^{\tau}\boldsymbol{x})\right\}$ is the partition function. Thus, according to Eqn. (23), the new model $P^{\tau+1}(\boldsymbol{y}|\boldsymbol{x})$ is

$$\begin{aligned} &P^{\tau+1}(\boldsymbol{y}|\boldsymbol{x}) \\ &= \tfrac{1}{Z^{\tau+1}(\boldsymbol{x})} \exp\left\{\boldsymbol{y}^T\left((\boldsymbol{b}^{\tau} + \boldsymbol{b}^{\star}) + (\boldsymbol{R}^{\tau} + \boldsymbol{R}^{\star})\boldsymbol{y} + (\boldsymbol{W}^{\tau} + \boldsymbol{W}^{\star})\boldsymbol{x}\right)\right\} \end{aligned} \tag{31}$$

We can find $P^{\tau+1}(\boldsymbol{y}|\boldsymbol{x})$ has the same probabilistic form like $P^{\tau}(\boldsymbol{y}|\boldsymbol{x})$ except their parameters have been adapted as

$$\begin{aligned} \boldsymbol{b}^{\tau+1} &\leftarrow \boldsymbol{b}^{\tau} + \boldsymbol{b}^{\star} \\ \boldsymbol{R}^{\tau+1} &\leftarrow \boldsymbol{R}^{\tau} + \boldsymbol{R}^{\star} \\ \boldsymbol{W}^{\tau+1} &\leftarrow \boldsymbol{W}^{\tau} + \boldsymbol{W}^{\star} \end{aligned} \tag{32}$$

Therefore, such an online adaptation can then be iterated in the same manner in each iteration. Here, the initial model P^0 can be started with the parameters $\boldsymbol{b}^0 = 0$, $\boldsymbol{R}^0 = 0$, $\boldsymbol{W}^0 = 0$.

To the best of our knowledge, we are the first to develop an online learner for multi-lable classfication problem, althought there exist some incremental or online learners for the binary classfication which do not model the correlations between different labels [25] [26] [27].

IV. Implementation Details

In this section, we discuss some implementation details about the two dimensional active learning with the proposed online learner.

A. Kernelization

Note that the model in Eqn. (23) is linear and can be effective on a set of samples that vary linearly. However, it will fail to capture the structure of the feature space if the variations among the samples are nonlinear. But image classification is in this case when one is trying to extract features from image categories that vary in their appearance, illumination conditions and complex background clutters. Therefore, a nonlinear version is required to classify the images based on their nonlinear structure in their feature space.

Here we extend the model in Eqn. (23) to a nonlinear one so that the powerful kernel method can be adopted. A transformation ψ maps samples into a target space in which kernel function $k(\boldsymbol{x}', \boldsymbol{x})$ gives the inner product. We can rewrite Eqn. (23) as

$$\begin{aligned} &P^{\tau+1}(\boldsymbol{y}|\boldsymbol{x}) \\ &= \tfrac{1}{Z^{\tau+1}(\boldsymbol{x})} P^{\tau}(\boldsymbol{y}|\boldsymbol{x}) \exp\left(\boldsymbol{y}^T(\boldsymbol{b} + \boldsymbol{R}\boldsymbol{y}) + \boldsymbol{y}^T\psi(\boldsymbol{W}) \cdot \psi(\boldsymbol{x})\right) \end{aligned} \tag{33}$$

where $\psi(\boldsymbol{W})$ is the mapped weighting matrix. According to the Representer Theorem, the optimal weighting vector of the single-label problem is a linear combination of samples. In the proposed multi-label setting, the mapped weighting matrix $\psi(\boldsymbol{W})$ can still be written as a linear combination of $\psi(\boldsymbol{x}_i)$ except that the combination coefficients are vectors instead of scalars, i.e.

$$\begin{aligned} &\psi(\boldsymbol{W}) = \textstyle\sum_{i=1}^{n} \theta(\boldsymbol{x}_i)\psi^T(\boldsymbol{x}_i) \\ &= \begin{bmatrix} \theta(\boldsymbol{x}_1) & \theta(\boldsymbol{x}_2) & \cdots & \theta(\boldsymbol{x}_n) \end{bmatrix} \begin{bmatrix} \psi^T(\boldsymbol{x}_1) \\ \psi^T(\boldsymbol{x}_2) \\ \vdots \\ \psi^T(\boldsymbol{x}_n) \end{bmatrix} \\ &= \Theta \cdot \begin{bmatrix} \psi^T(\boldsymbol{x}_1) \\ \psi^T(\boldsymbol{x}_2) \\ \vdots \\ \psi^T(\boldsymbol{x}_n) \end{bmatrix} \end{aligned} \tag{34}$$

where the summation is taken over the samples in the training set. $\theta(\boldsymbol{x}_i)$ is a coefficient vector and Θ is a $m \times n$ matrix in which each row is the weighting coefficients for each label. Accordingly, we have

$$\begin{aligned} &\psi(\boldsymbol{W}) \cdot \psi(\boldsymbol{x}) \\ &= \Theta \cdot \begin{bmatrix} k(\boldsymbol{x}_1, \boldsymbol{x}) & \cdots & k(\boldsymbol{x}_n, \boldsymbol{x}) \end{bmatrix}^T \\ &= \Theta \cdot k(\boldsymbol{x}) \end{aligned} \tag{35}$$

and

$$\begin{aligned} &P^{\tau+1}(\boldsymbol{y}|\boldsymbol{x}) \\ &= \tfrac{1}{Z^{\tau+1}(\boldsymbol{x})} P^{\tau}(\boldsymbol{y}|\boldsymbol{x}) \exp\left(\boldsymbol{y}^T(\boldsymbol{b} + \boldsymbol{R}\boldsymbol{y} + \Theta k(\boldsymbol{x}))\right) \end{aligned} \tag{36}$$

where $k(\boldsymbol{x}) = \begin{bmatrix} k(\boldsymbol{x}_1, \boldsymbol{x}) & \cdots & k(\boldsymbol{x}_n, \boldsymbol{x}) \end{bmatrix}^T$ is a $n \times 1$ vector and it can be seen as a new representation of sample $\boldsymbol{x}$. Correspondingly, with the identity $||\phi(\boldsymbol{W})||_F^2 = tr(\phi(\boldsymbol{W})\phi(\boldsymbol{W})^T) = tr(\Theta K \Theta^T)$ the Lagrangian function (27) can be rewritten as

$$\begin{aligned} &\mathcal{L}(\boldsymbol{b}, \boldsymbol{R}, \Theta) = \left\langle \boldsymbol{y}^T(\boldsymbol{b} + \boldsymbol{R}\boldsymbol{y} + \Theta \cdot k(\boldsymbol{x})) - Z^{\tau+1}(\boldsymbol{x}) \right\rangle_{\tilde{P}(\boldsymbol{x},\boldsymbol{y})} \\ &- \tfrac{\alpha_b}{2n}||\boldsymbol{b}||_2^2 - \tfrac{\alpha_R}{2n}||\boldsymbol{R}||_F^2 - \tfrac{\alpha_W}{2n} tr(\Theta K \Theta^T) \end{aligned} \tag{37}$$

where $K = [k(\boldsymbol{x}_i, \boldsymbol{x}_j)]_{n \times n}$ is the kernel matrix. By maximizing (37), we can estimate the optimal parameters $\boldsymbol{b}^{\star}$, $\boldsymbol{R}^{\star}$, $\Theta^{\star}$ in this kernelization formulation.

Here, we do not assume any specific form of the old model $P^{\tau}(\boldsymbol{y}|\boldsymbol{x})$. Similar to the discussion in the above subsection, we can assume $P^{\tau}(\boldsymbol{y}|\boldsymbol{x})$ has the following form

$$P^{\tau}(\boldsymbol{y}|\boldsymbol{x}) = \tfrac{1}{Z^{\tau}(\boldsymbol{x})} \exp\left(\boldsymbol{y}^T(\boldsymbol{b}^{\tau} + \boldsymbol{R}^{\tau}\boldsymbol{y} + \Theta^{\tau}k^{\tau}(\boldsymbol{x}))\right) \tag{38}$$

Accordingly, the new model $P^{\tau+1}(\boldsymbol{y}|\boldsymbol{x})$ can be

$$\begin{aligned} &P^{\tau+1}(\boldsymbol{y}|\boldsymbol{x}) = \tfrac{1}{Z^{\tau+1}(\boldsymbol{x})} \\ &\cdot \exp\left\{\boldsymbol{y}^T\left((\boldsymbol{b}^{\tau} + \boldsymbol{b}^{\star}) + (\boldsymbol{R}^{\tau} + \boldsymbol{R}^{\star})\boldsymbol{y} + [\Theta^{\tau}\ \Theta^{\star}] \begin{bmatrix} k^{\tau}(\boldsymbol{x}) \\ k(\boldsymbol{x}) \end{bmatrix}\right)\right\} \end{aligned} \tag{39}$$

The above new model has the similar probabilistic form as the old one except the parameters have been adapted as

$$\begin{aligned} \boldsymbol{b}^{\tau+1} &\leftarrow \boldsymbol{b}^{\tau} + \boldsymbol{b}^{\star} \\ \boldsymbol{R}^{\tau+1} &\leftarrow \boldsymbol{R}^{\tau} + \boldsymbol{R}^{\star} \\ \Theta^{\tau+1} &\leftarrow [\Theta^{\tau}\ \Theta^{\star}] \end{aligned} \tag{40}$$

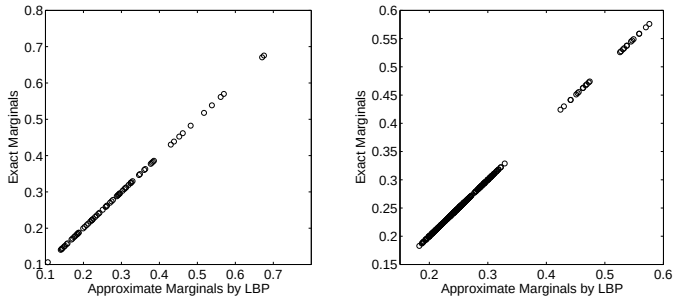

(a) six Labels (b) 14 Labels

Fig. 3. Correlation plots between the exact and approximate marginals $P^{\tau+1}(y_i|\boldsymbol{x})$ and $P^{\tau+1}(y_i, y_j|\boldsymbol{x})$ for the proposed fully-connected graphical models with the different number of labels: (a) six labels and (b) 14 labels.

and the new representation for the sample $\boldsymbol{x}$ is

$$k^{\tau+1}(\boldsymbol{x}) \leftarrow \begin{bmatrix} k^{\tau}(\boldsymbol{x}) \\ k(\boldsymbol{x}) \end{bmatrix} \tag{41}$$

With the above equations, we can recursively update the parameters of the probabilistic model once the new samples are acquired. As stated in Section I, such an online learning algorithm can be much more efficient than the traditional retraining algorithm, especially when the number of the accumulated samples grows rapidly.

B. Incomplete Labeling

Given the partially labeled training set constructed by 2DAL (see Figure 1), we can handle the incomplete labels by integrating out the unlabeled part yielding the marginal distribution of the labeled part $P^{\tau+1}(y_{L(\boldsymbol{x})}|\boldsymbol{x}) = \sum_{y_{U(\boldsymbol{x})}} P^{\tau+1}(y_{U(\boldsymbol{x})}, y_{L(\boldsymbol{x})}|\boldsymbol{x})$. But this form will lead to intractable computations and a nonconvex objective function which results in a local optimum solution. Instead, we use the Expectation Maximization (EM) algorithm [28] to solve this incomplete labeling problem. EM algorithm can greatly reduce the computational cost. As stated in many existing literatures [29], EM iteratively optimizes a series of local lower-bounds to the original objective function obtained by marginalizing over all the unlabeled part. Such local lower bounds are convex and thus the global optimum can be found at each M-step for these convex bounds. These related works prove these local lower-bounds can approximate the true nonconvex objective function well enough and thus EM can result in a good solution.

E-Step: Given the current t-th step parameter estimation $\boldsymbol{b}_t, \boldsymbol{R}_t, \Theta_t$, the $\mathcal{T}$-function (i.e., the expectation of the Lagrangian Eqn. (37) under the current parameters given the labeled part) can be written as

$$\begin{aligned}&\mathcal{T}(\boldsymbol{b}, \boldsymbol{R}, \Theta|\boldsymbol{b}_t, \boldsymbol{R}_t, \Theta_t)\\ &= \left\langle E_{U(\boldsymbol{x})|L(\boldsymbol{x});\boldsymbol{b}_t,\boldsymbol{R}_t,\Theta_t} \boldsymbol{y}^T(\boldsymbol{b} + \boldsymbol{R}\boldsymbol{y} + \Theta k(\boldsymbol{x})) - Z^{\tau+1}(\boldsymbol{x}) \right\rangle_{\widetilde{P}(\boldsymbol{x},\boldsymbol{y})}\\ &- \tfrac{\alpha_b}{2n}||\boldsymbol{b}||_2^2 - \tfrac{\alpha_R}{2n}||\boldsymbol{R}||_F^2 - \tfrac{\alpha_W}{2n} tr(\Theta K \Theta^T)\end{aligned} \tag{42}$$

where $E_{U(\boldsymbol{x})|L(\boldsymbol{x});\boldsymbol{b}_t,\boldsymbol{R}_t,\Theta_t}$ is the expectation operator given the current estimated conditional probability $P^{\tau+1}(y_{U(\boldsymbol{x})}|y_{L(\boldsymbol{x})}, \boldsymbol{x}; \boldsymbol{b}_t, \boldsymbol{R}_t, \Theta_t)$.

M-Step: Update the parameters by minimizing $\mathcal{T}$-function:

$$\boldsymbol{b}_{t+1}, \boldsymbol{R}_{t+1}, \Theta_{t+1} = \arg\max_{\boldsymbol{b},\boldsymbol{R},\Theta} \mathcal{T}(\boldsymbol{b}, R, \Theta|\boldsymbol{b}_t, \boldsymbol{R}_t, \Theta_t) \tag{43}$$

The derivatives of $\mathcal{T}$-function with respect to its parameters $\boldsymbol{b}, \boldsymbol{R}, \Theta$ is

$$\begin{aligned}\frac{\partial \mathcal{T}}{\partial b_i} &= \left\langle E_{y_i|L(\boldsymbol{x});\boldsymbol{b},\boldsymbol{R},\Theta} y_i \right\rangle_{\widetilde{P}(\boldsymbol{x},\boldsymbol{y})} - \langle y_i \rangle_{P^{\tau+1}(\boldsymbol{x},\boldsymbol{y})} - \tfrac{\alpha_b}{n} b_i,\\ \frac{\partial \mathcal{T}}{\partial R_{ij}} &= \left\langle E_{y_i,y_j|L(\boldsymbol{x});\boldsymbol{b},\boldsymbol{R},\Theta} y_i y_j \right\rangle_{\widetilde{P}(\boldsymbol{x},\boldsymbol{y})} - \langle y_i y_j \rangle_{P^{\tau+1}(\boldsymbol{x},\boldsymbol{y})} - \tfrac{\alpha_R}{n} R_{ij}\\ \frac{\partial \mathcal{T}}{\partial \Theta_{il}} &= \left\langle E_{y_i|L(\boldsymbol{x});\boldsymbol{b},\boldsymbol{R},\Theta} y_i k(\boldsymbol{x}_l, \boldsymbol{x}) \right\rangle_{\widetilde{P}(\boldsymbol{x},\boldsymbol{y})} - \langle y_i k(\boldsymbol{x}_l, \boldsymbol{x}) \rangle_{P^{\tau+1}(\boldsymbol{x},\boldsymbol{y})}\\ &- \tfrac{\alpha_W}{n} \textstyle\sum_{k=1}^{n} \Theta_{ik} k(\boldsymbol{x}_k, \boldsymbol{x}_l)\end{aligned} \tag{44}$$

Similarly, with the above derivatives, L-BFGS [24] can then be applied to maximize (43).

C. Efficient Inference

When computing the derivatives (43), we need to compute the marginal distributions of $P^{\tau+1}(\boldsymbol{y}|\boldsymbol{x})$ over the fully-connected graph on the labels, such as $P^{\tau+1}(y_i|\boldsymbol{x})$ and $P^{\tau+1}(y_i, y_j|\boldsymbol{x})$. On the other hand, these marginal distributions are also required to compute the mutual information used in 2DAL (see Eqn. (9)). It is known that the computational cost will be intractable with the increment of the label number m, and this limits the applicability of the algorithm. Fortunately, there exist many efficient algorithms to compute these marginals, such as Markov Chain Monte Carlo (MCMC) [30], Loopy Belief Propagation (LBP) [31] and Expectation Propagation (EP) [32]. Here, we adopt the widely-used LBP to compute these marginal distributions. To apply the LBP, we need to provide the local evidences and potential functions. From the kernelized model $P^{\tau+1}(\boldsymbol{y}|\boldsymbol{x})$ in Eqn. (36) we can find its local evidences as

$$\Psi^{\tau+1}(y_i) \propto \exp\left\{ b_i^{\tau+1} y_i + \sum_{k=1}^{n} \Theta_{ik}^{\tau+1} y_i k^{\tau+1}(\boldsymbol{x}_k, \boldsymbol{x}) \right\} \tag{45}$$

and its potentials

$$\Psi^{\tau+1}(y_i, y_j) \propto \exp\left\{ R_{ij}^{\tau+1} y_i y_j \right\} \tag{46}$$

By propagating the above local evidences and potentials, LBP can then be used to efficiently compute all the marginal distributions simultaneously. For detailed LBP algorithm, please refer to [31].

Murphy et al. [33] have conducted an empirical study and they find that LBP converges well on a variety of graphical models. Once LBP converges, the obtained marginals can give a good approximation to the exact marginals. Similarly, in order to verify this conclusion on the model represented by Eqn. (42) and (43), we also conduct an empirical study to test the convergence of LBP on the two fully-connected graphical models with six and 14 labels. A set of test samples from the datasets in following experiment section VI are used as observations $\boldsymbol{x}$. Then the posterior marginals $P^{\tau+1}(y_i|\boldsymbol{x})$ and $P^{\tau+1}(y_i, y_j|\boldsymbol{x})$ are computed by LBP. Experiments show LBP converges in less than two iterations over all these test samples and figure 3 illustrates the correlation between the exact and approximate marginals. The results illustrate LBP converges to good

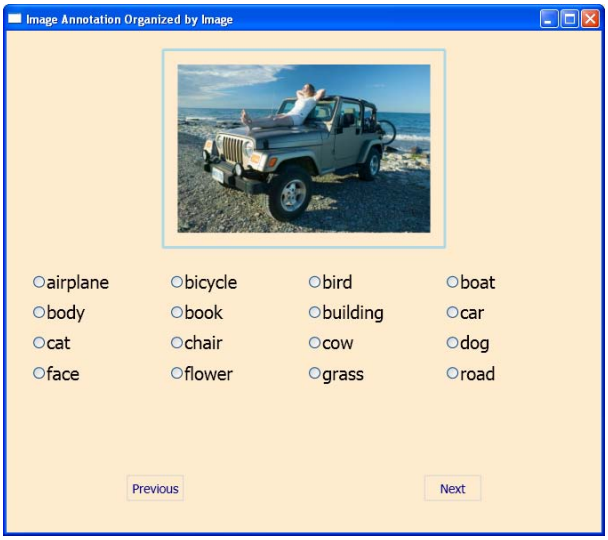

Fig. 4. The user interface that organizes image annotation by image. Users annotate all the concepts simultaneously for each image before proceeding to the next one.

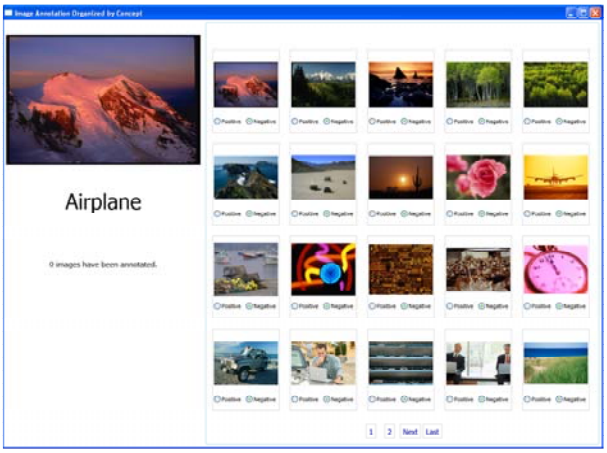

Fig. 5. The user interface that organizes image annotation by concept. Users annotate all the images exhaustively with a concept before proceeding to the next one.

approximate marginals w.r.t. the exact one. The absolute errors between these approximate marginals and the exact ones are 8.50×10^{-6} and 1.31×10^{-5} on average in these two graphical models, respectively. If the typical LBP does not converge in some special cases, there also exist methods of preventing LBP from oscillation. For example, [33] proposes to use "momentum" by replacing the current messages with a weighted combination of the current message and previous ones, which can significantly reduce the chance of oscillation.

V. User Interface for Annotating Images

An effective User Interface (UI) is a critical factor to improve the interaction efficiency between human beings and computers when annotating images. Traditionally, the image annotation interface is designed to annotate all the concepts simultaneously for each image before proceeding to the next one (see figure 4 for an example of this interface). However we argue such an interface is not the most suitable

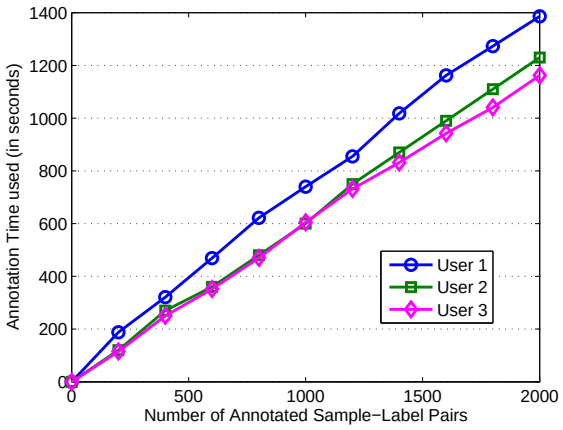

Fig. 6. User study for the user interface for image annotation organized by concept.

choice to annotate images with multiple labels, because the annotators must switch their minds between different concepts to annotate these images and it can exhaust annotators' energy more quickly. An alternative choice is to annotate all the images exhaustively with a concept before proceeding to the next one. In this interface, annotators can focus on only one concept at one time so that they can quickly browse a group of images to judge if the concept exists in these images. That is because the vision system of human beings can rapidly respond to visual information of multiple images in a very short time. For example, given the images in an annotation interface illustrated in Figure 5, annotators can find which images contain the concept "airplane" in a rather short time, instead of having to judge these images one by one. In contrast, in the traditional annotation interface of Figure 4, annotators cannot focus on one concept to annotate all the images before proceeding to the next concept, and it reduces the annotators' efficiency. Therefore, we organize the image annotation by concept as illustrated in Figure 5 rather than by image as in Figure 4. In addition to the consideration of annotation efficiency, organizing annotation by concept can also lead to more accurate and complete annotation than annotating all concepts for each image simultaneously. Past experience has shown that the latter can cause many concepts to be missed (i.e., causing false negative labeling) [34].

In the user interface that organizes image annotation by concept as Figure 5, the annotation workload is proportional to the number of sample-label pairs rather than the number of distinct images associated with these pairs, because the time used to annotate a certain concept for an image (i.e., a sample-label pair) can be assumed to be a constant on average. Therefore in this interface, it is reasonable to compare the performances of 2DAL against the other active learning approaches under the same number of selected sample-label pairs as the basic unit to measure the annotation costs.

To verify the assumption that image annotation workload is proportional to the number of label-sample pairs rather than the number of distant images in the annotation interface organized by concept, we conduct a user study on this

User ID	Organizing annotation by image	Organizing annotation by concept
1	3660	1386
2	3138	1230
3	3138	1162

TABLE I
COMPARISON BETWEEN THE INTERFACE ORGANIZING ANNOTATION BY IMAGE AND THAT BY CONCEPT.

Class	Total	Class	Total
Beach	369	Beach+Mountain	38
Sunset	364	Foliage+Mountain	13
Foliage	360	Field+Mountain	75
Field	327	Field+Foliage+Mountain	1
Beach+Field	1	Urban	405
Foliage+Field	23	Beach+Urban	19
Mountain	405		

TABLE II
Scene DATA SET

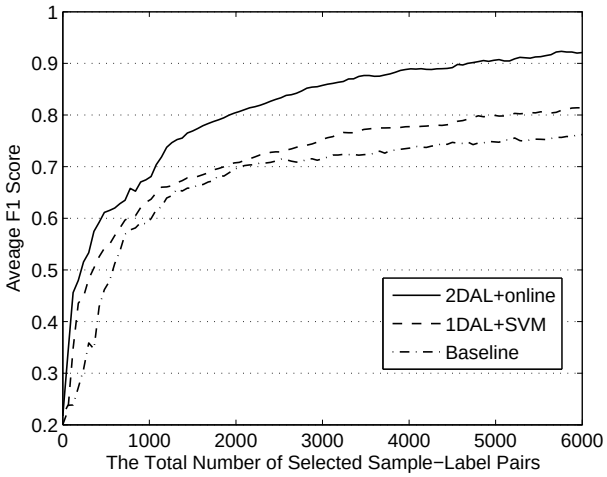

Fig. 7. The performance of three active learning strategies over the *Scene* data set.

Class	2DAL+online	1DAL+SVM	Baseline
Beach	0.9523	0.8652	0.6744
Sunset	0.9916	0.9421	0.9002
Fall Foliage	0.9887	0.9338	0.8927
Field	0.9588	0.8813	0.8071
Mountain	0.7806	0.6457	0.6122
Urban	0.8534	0.6162	0.6856

TABLE III
$F1$ SCORES AFTER 100 ITERATIONS ON SIX SCENE CATEGORIES.

interface. Each of three users annotated 200 sample-label pairs that are associated with *varying* number of images in each step. This step was repeated ten times, yielding 2,000 sample-label pairs per user. First, we compare the annotation efficiency on the interface organizing annotation by image as Figure 4 and that by concept as Figure 5. In table I, we report the time used on these two interfaces by these three users. Obviously organizing annotation by concept is much more efficient than that by image and thus we will adopt the former one to annotate images. Second we verify the image annotation workload is related to the number of label-sample pairs on the interface as Figure 5. Figure 6 illustrates the linear relationship between annotation time and the number of annotated sample-label pairs on this interface. We can find the annotation time is proportional to the number of annotated sample-label pairs. It verifies the annotation workload can be measured by the number of sample-label pairs. Therefore in the later experiments, we will compare the performances of different active learning approaches under the same number of sample-label pairs.

VI. EXPERIMENTS ON TWO BENCHMARK DATASETS

In this section, we conduct experiments on two publicly available datasets to evaluate the proposed algorithm.

A. Natural scene classification

This natural scene data set is first used in a previous research on the multi-label image scene classification problem [13][1]. It contains $2,407$ natural images belonging to one or more of six natural scene categories including beach, sunset, fall foliage, field, mountain, and urban. Since the data sets are multi-labeled, there are $14,442$ sample-label pairs in this set.

An image is first converted into CIE Luv color space and then the first and second color moments (mean and variance) are extracted over a 7×7 grid on the image. The end result is a $49 \times 2 \times 3 = 294$ dimension feature vector [13].

In this experiment, we compare the following three active learning strategies:

1 The proposed 2DAL strategy (2DAL+online): using the proposed sample-label pair selection criterion in Section II-B, associated with the online adaptation statistical model (23) as the underlying classifier.

2 1D active learning strategy (1DAL+SVM): using the mean-max loss active learning strategy that has been proposed in [12] on multi-label active learning. As stated in Section I, this strategy selects only along the sample dimension. It does not take advantage of the label correlations to reduce human labeling cost. To the best of our knowledge, there exist very limited literatures on the multi-label active learning [12] [14] and 1DAL here is among these methods. All these existing methods are 1D-style active learning which only selects samples rather than sample-label pairs. Thus we compare with the existing 1DAL method to verify the effectiveness of the proposed 2DAL.

3 Baseline: the random strategy - selecting the sample-label pairs at random. For the sake of fair comparison with the proposed 2DAL, we also use the online adaptation learner (23) in Section III as the classifier.

[1]This data set is publicly available at http://www.csie.ntu.edu.tw/˜cjlin/libsvmtools/datasets/multilabel.html#scene-classification.

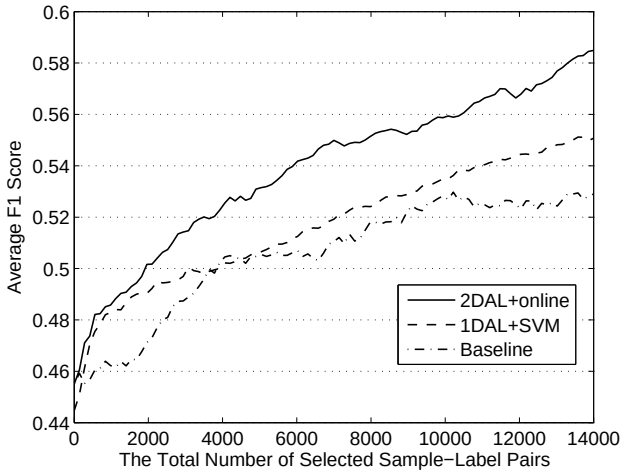

Fig. 8. The performance of three active learning strategies over the *Yeast* data set.

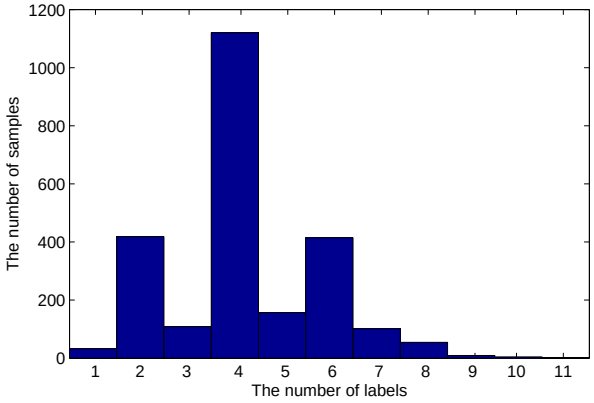

Fig. 9. The distribution of the label numbers for the gene samples on the *Yeast* data set.

We use the average $F1$ score over all different labels for performance evaluation, i.e., $F1 = \frac{2rp}{r+p}$ where p and r are precision and recall respectively. It is the harmonic mean of precision and recall. In statistics, the $F1$ score measures a test's accuracy and has been widely used in information retrieval. For this Scene data set, we use 241 (10%) images as the initial training set. In each iteration, 60 sample-label pairs are selected by the 2DAL. Note that, for 1DAL, it requests annotation on the basis of samples rather than sample-label pairs, so in each iteration, it selects 10 images for annotating all the six labels or equivalently 60 image-label pairs. The average $F1$ score is then computed over all the remaining unlabeled data. In Figure 7, we show the performance of these three strategies versus the number of the selected sample-label pairs. The proposed 2DAL has the best performance in all the iterations. With the number of selected pairs increasing, the improvement becomes more and more significant. Table III compares the $F1$ scores after 100 iterations over all the six scene categories, which illustrates 2DAL outperforms the other strategies on all the labels. In particular, the improvement is obvious on "Urban". Such an improvement is obtained by considering its significant correlations with other labels, such as "Mountain" and "Fall foliage". It confirms 2DAL can obviously improve the classification performance.

Note that in the above comparison, the performances of different active learning approaches are compared under the same number of sample-label pairs. As indicated in Section V, the labor cost for image annotation is linear to the number of sample-label pairs in the user interface as Figure 5. Therefore it is reasonable to prove the superiority of an active learning algorithm if it can improve the classification accuracy with the same number of selected sample-label pairs.

B. Gene Classification

The second benchmark data set is the Yeast data set [11] which consists of micro-array expression data and phylogenetic profiles with 2,417 genes. Each gene in the set belongs to one or more of 14 different functional classes[2], yielding $33,838$ sample-label pairs. Figure 9 illustrates the distribution of the label numbers for the gene samples on this Yeast data set. The detailed description about this biological data set can be found in [35].

In the experiment, 242 (10%) genes with their labels are used as the initial training set. In each iteration, 140 sample-label pairs are selected. Similar to the above subsection, 1DAL selects 10 samples for annotating all their labels, which is 140 sample-label pairs. Figure 8 compares the performance of the three strategies.

From the above two experiments, we have observed:

1 Given a fixed number of annotations, 2DAL outperforms 1DAL over all the active learning iterations. This is because the former considers both sample and label uncertainty for selecting sample-label pair, while 1DAL only considers the sample uncertainty. Therefore, the informative label correlations associated with each sample can help to reduce the expensive human labor needed to construct the labeled pool.

2 The proposed 2DAL gives good performance on diverse data sets, ranging from natural scenes to gene images. This is an important character of a good algorithm to be used in real-world applications.

VII. Real-world image classification

In this section, we evaluate the proposed online active learning algorithm on a real-world image data set. This data set is obtained from an image sharing website - Corbis (http://www.corbis.com). Figure 10 illustrates the snapshot of this website. We construct a realistic image data set from this website. This data set contains 28,868 images uploaded by the users. Each image is annotated from a set of 23 labels. Table IV shows these 23 labels and the image numbers associated with them. Figure 11 illustrates some example images and their associated labels. We can find these real-world images are usually annotated by multiple labels.

[2]This data set is publicly available at http://www.csie.ntu.edu.tw/~cjlin/libsvmtools/datasets/multilabel.html#yeast

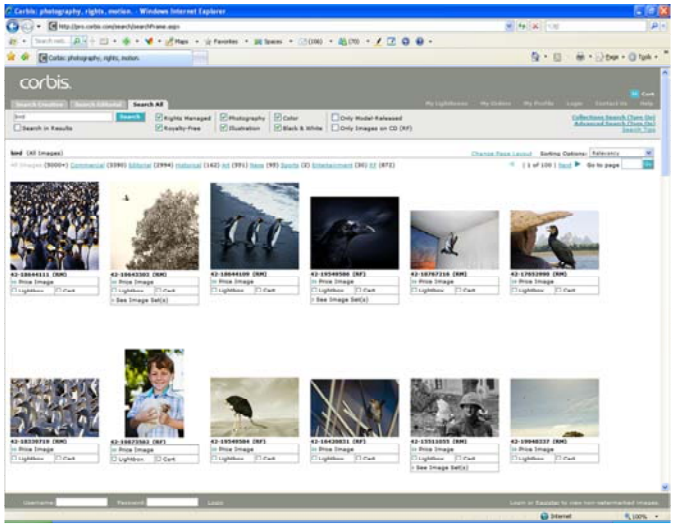

Fig. 10. Snapshot of the image sharing Website - Corbis: http://www.corbis.com. This website provides a service of searching the images by their keywords. Such a service proposes the requirement to automatically annotate the labels of the images. In this example, this service returns the images that have labeled by the keyword "bird".

Label Name	Total	Label Name	Total
airplane	350	face	998
bicycle	5146	flower	512
bird	13899	grass	5178
boat	1617	road	956
body	4532	sheep	3455
book	1200	sign	1262
building	8736	sky	1091
car	2808	tree	235
cat	1041	water	175
chair	3910	mountain	1225
cow	2454	horse	126
dog	1462		

TABLE IV
THE NUMBER OF IMAGES ASSOCIATED WITH EACH LABEL IN THE CORBIS DATA SET.

Different from the global features extracted from the images in the *Scene* data set [13], we extract the dense local features as suggested in [36]. In more detail, each image is first normalized into 256×256 pixels and then represented by a two dimensional array of local patches. Each local patch has 16×16 pixels over a grid with spacing of 8 pixels. We extract three kinds of features for each patch as follows

- Color moments (9 dim) - the first, second and third color moments in each component of CIE Luv color space.
- Co-occurrence texture (16 dim) - it computes the occurrence distribution of the 16 different patterns in a local patch.
- SIFT descriptor - the 128-dimensional SIFT descriptor is processed by principal component analysis (PCA) to reduce its dimensionality to 50.

With the above grid-based two dimensional representation of images, we can compute a kernel between the images into the proposed algorithm as depicted in Section IV. In this paper, we use the joint appearance-spatial kernel proposed in our previous work [37]. This kernel is based on the distance between two Dependent Tree - HMMs (DT-HMMs) [38] - a variant 2-Dimensional Hidden Markov Model (2DHMM). Figure 12 illustrates an example of DT-HMM. With this structure of 2D Markov fields on the images, we can tractably compute a tighter upper bound of the Kullback-Leibler Divergence (KLD) between these DT-HMMs. Accordingly a kernel can be defined on the basis of

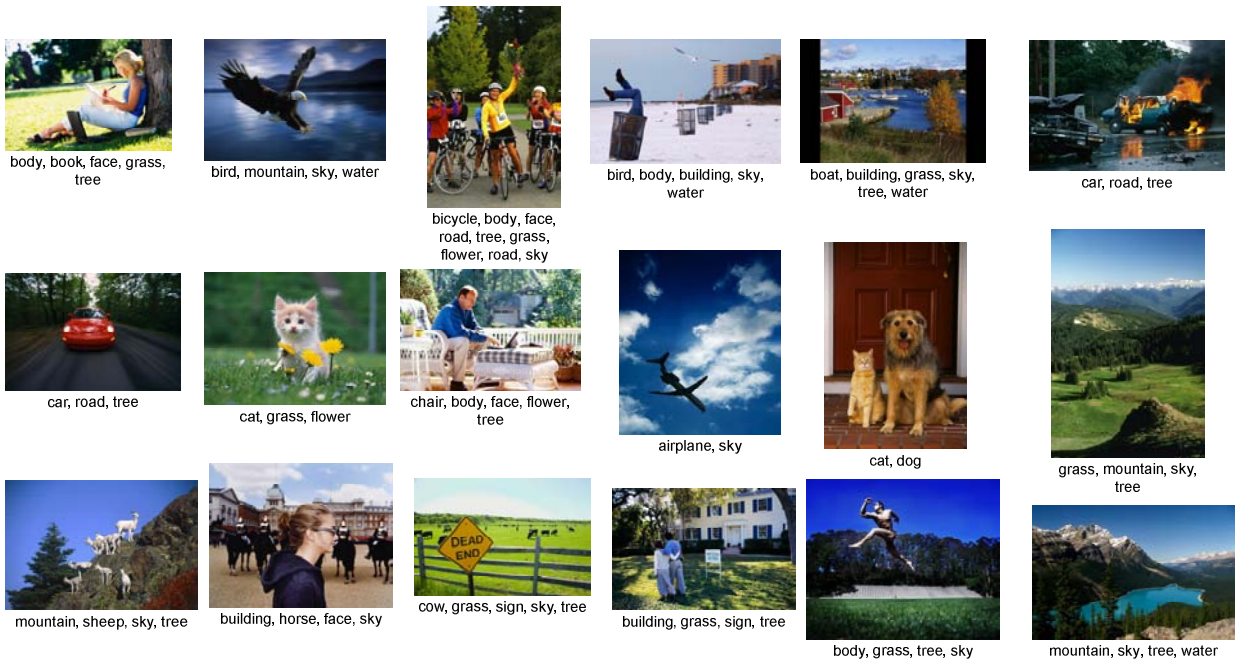

Fig. 11. Some examples of the images acquired from the Corbis website and their associated labels. From these examples, we can find most of the real-world images can be annotated by multiple labels simultaneously.

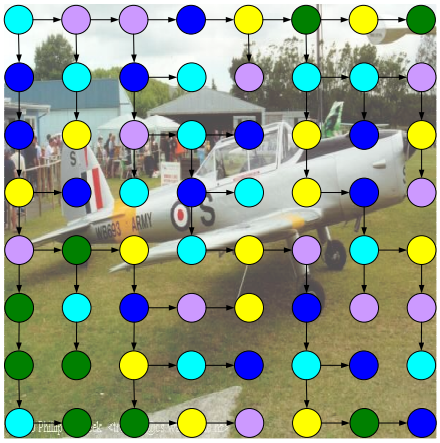

Fig. 12. An example of Dependent Tree Hidden Markov Model (DT-HMM) [38]. A joint appearance-spatial kernel can be defined by computing the Kullback-Leibler Divergence between these DT-HMMs [37]. This kernel can capture the image similarity of both the appearance and the spatial structure in a unifying formulation.

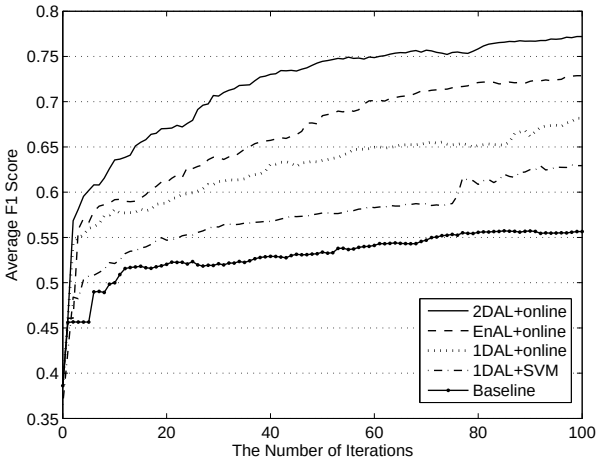

Fig. 13. Comparison of various active learning approaches. (1) 2DAL+online: using 2DAL strategy with the online learner;(2) EnAL+online: using the most uncertainty criterion with the online learner; (3) 1DAL+online: using 1DAL strategy with online learner; (4) 1DAL+SVM: using 1DAL strategy with SVM learner; (5) Baseline: using the random strategy.

the KLD by exponentiating them. The reason that we choose this kernel in this paper is twofolds. First, different from many other kernels which only measure the appearance similarity between images, this kernel can also measure the spatial similarity simultaneously. In fact, the spatial structure of local patches is rather important cue for image classification problem. Thus a joint appearance-spatial kernel like this one can bring significant advantage during the classification. Second, we extract three different kinds of feature modalities as above. Effective fusion of these modalities in classification attracts much research attentions [39]. This kernel algorithm can compute the similarity measure between images over all the modalities simultaneously without a late fusion [39] of the classification results on each single modality. The details about computing these kernels can be found in [37].

A. Performance Comparison with Previous Work

In this experiment, we also compare the proposed 2DAL+online approach with 1DAL+SVM and Baseline like the experiments on the benchmark data sets.

At the beginning, we use 10,000 images as the initial training set. In each iteration, 1DAL selects 100 images for annotating all 23 labels, containing $100 \times 23 = 2,300$ sample-label pairs. Equivalently 2DAL and the random baseline request annotation of 2,300 sample-label pairs. A separate set of 5,000 samples are used as validation set and the average $F1$ score is computed on it to compare the performances of different approaches. Such active learning iterations are repeated 100 times. Figure 13 illustrates the performance of the three active learning strategies. We can find that

1 The 2DAL+online has the best performance of all the three strategies in the all 100 iterations.

2 After 100 iterations, $F1$ score of the 2DAL+online obtains 0.772 in contrast to 0.629 for 1DAL+SVM and 0.557 for the baseline. In other words, 2DAL+online gains 22.7% and 38.6% improvements compared to 1DAL+SVM and the baseline in terms of $F1$ score.

B. Does label correlation really help in 2DAL?

To show the superiority of the proposed 2DAL+online, we conduct an experiment which also selects the sample-label pairs like 2DAL+online but ignores the label correlations. As presented in Eqn. (10), the 2DAL strategy can be divided into two terms: one is the self entropy for the selected sample-label pair and the other is its correlations with the other labels. If we ignore the second term, this strategy reduces to an algorithm similar to the traditional active learning approach which only selects the most "informative" pair but ignores the label correlations. Here we test the strategy without the second term to see if the label correlation really contributes to the performance improvement. We call this strategy EnAL (Entropy based Active Learning) since it only uses the first entropy term. For the sake of fair comparison with 2DAL, we also use the online learner as the underlying classifier in EnAL. The experimental results are illustrated in Figure 13 denoted by EnAL+online. From this illustration, we can observe that

- 2DAL+online outperforms EnAL+online in all the 100 iterations. This result proves utilizing the label correlations in active learning is a better strategy.

C. Where the superiority of 2DAL+online comes from, 2DAL selection strategy or online learner?

It is worthy of noting that 2DAL+online is based on the proposed online learner for the multi-label classification in Section III while 1DAL+SVM proposed in [12] depends on SVM learner. We conduct extra experiments here to testify whether the performance gain in 2DAL+online comes from the 2DAL selection strategy proposed in Section II or from the online learner developed in Section III. Three compared experiments are conducted as

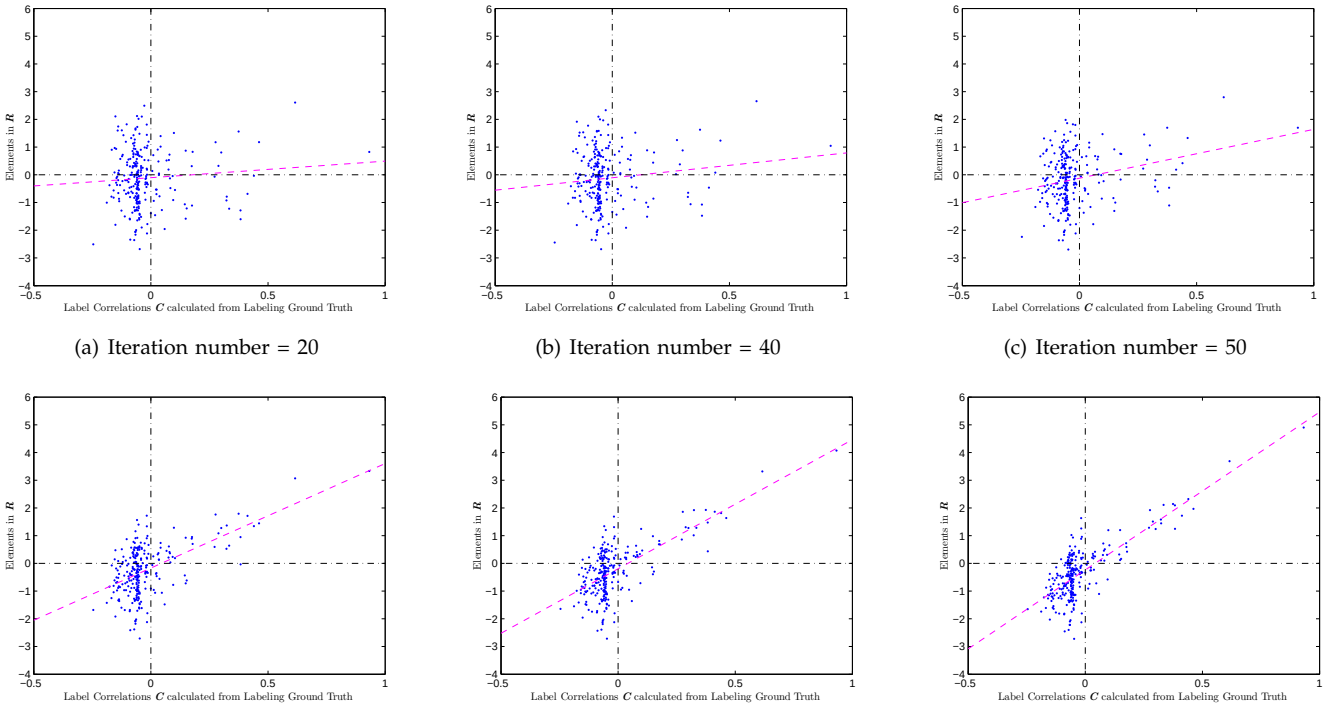

(a) Iteration number = 20 (b) Iteration number = 40 (c) Iteration number = 50

(d) Iteration number = 60 (e) Iteration number = 80 (f) Iteration number = 100

Fig. 14. The horizontal axis in each figure denotes the linear correlation coefficients $\boldsymbol{C}$ between the labels calculated from the labeling ground truth. Here, the linear correlation coefficients can be seen the label correlation ground truth. The vertical axis denotes the elements in $\boldsymbol{R}$. The dashed line is the linear regression from the points in figures. These figures illustrate the relation between the label correlation ground truth (horizontal axis) and the corresponding elements in $\boldsymbol{R}$ (vertical axis). With the increment of the iteration number, the compliance between the label correlation ground truth $\boldsymbol{C}$ and the elements in $\boldsymbol{R}$ becomes more and more significant. That is to say, a large C_{ij} usually has a large R_{ij} and vice versa. Such a compliance indicates the learned $\boldsymbol{R}$ can reflect the label correlations contained in the labeling ground truth of the Corbis data set.

1 Experiment I: it uses the online learner as the underlying statistical model and selects the sample-label pairs according to the proposed 2DAL strategy, which is 2DAL+online.
2 Experiment II: it also uses the online learner to train the label prediction model. However, it trains the classification model based on the image samples selected by 1DAL algorithm, that is 1DAL+online.
3 Experiment III: it uses the typical SVM as the underlying learner and the 1DAL strategy to select image samples, that is 1DAL+SVM.

The Experiment I and Experiment III are the same as the above 2DAL+online and 1DAL+SVM algorithms. In contrast, Experiment II combines the sample selection strategy in Experiment III and the online learner in Experiment I, i.e., in each iteration, the underlying learner in Experiment II is trained from the same selected data set in Experiment III. Thus we denote experiment II by 1DAL+online. Figure 13 compares the results of these three experiments. From these results, we can observe

1 Under the same underlying learner (i.e., online learner), 2DAL+online has the better performance than the 1DAL+online. It indicates 2DAL selection strategy is superior to the 1DAL selection strategy.
2 On the other hand, the underlying learners of 1DAL+online and 1DAL+SVM are trained on the same selected data set. It demonstrates the online learner for multi-label classification performs better than the typical SVM learner.

From the above observations, we can conclude that both the 2DAL selection strategy and the online learner contribute to the performance improvement of the proposed 2DAL algorithm (2DAL+online).

The superiority of the online learner is owed to the rich multi-label correlations in data set while the typical SVM learner ignores them. To demonstrate it, we illustrate the label correlations and their corresponding parameters in the matrix$\boldsymbol{R}$ in Figure 14. As discussed in Section III, each element R_{ij} in $\boldsymbol{R}$ is related to the label correlations between the label i and j. In Figure 14, we illustrate the label correlation ground truth C_{ij} in the horizontal axis versus the learned R_{ij} in the vertical axis $(1 \leq i < j \leq m)$. Here C_{ij} denotes the linear correlation coefficient between the label i and j calculated from the labeling ground truth over the whole data set. From this figure, we can find when the iteration number of active learning increases from $20, 40, 50, 60, 80$ until 100, the compliance between the label correlation ground truth $\boldsymbol{C}$ and the learned model parameter $\boldsymbol{R}$ becomes more and more significant. That is to say, a larger C_{ij} usually has a larger R_{ij} and vice versa. It confirms the learned model parameters $\boldsymbol{R}$ can reflect the real labeling correlations of the data set. In the other words, the online learner captures the label correlation evolution

Sample Selection	Computing Time
2DAL	149.5 seconds
1DAL	92.9 seconds

TABLE V
THE AVERAGE COMPUTING TIME USED FOR SAMPLE SELECTION IN EACH ITERATION

Learning Model	Computing Time
Online Learner	7.7 minutes
SVM	67.3 minutes

TABLE VI
THE AVERAGE COMPUTING TIME FOR UPDATING/RETRAINING MODELS IN EACH ITERATION.

contained in the selected sample-label pairs during the active learning procedure.

D. Computing Time

With the use of the proposed online learner, 2DAL is significantly more efficient than 1DAL which is based the offline SVM learner [12] . We summarize and compare the average computing time of the proposed 2DAL and 1DAL in each active learning iteration in Table V and VI. They are both performed on a 3.0GHz PC with 1GB RAM memory. The computing time consists of two parts. One part is for the sample selection in active learning and the other is for updating online model for 2DAL or retraining the SVM model for 1DAL. As for the computing time spent on sample selection, 2DAL strategy spends a little more time than 1DAL. They respectively use average 149.5 seconds and 92.9 seconds in each iteration. On the other hand, the online learner is much more efficient than the SVM in each iteration of updating/retraining their respective models. From Table VI, the online learner is nearly one order magnitude faster than the typical SVM, because it can be updated by only using the newly-acquired training samples while SVM needs to be retrained on all the training samples.

VIII. CONCLUSION

In this paper, we develop a two-dimensional multi-label active learning algorithm asking for human annotation along both sample and label dimensions. In contrast to the typical one-dimensional active learning algorithm that asks to annotate all the labels of the selected image samples, this 2DAL strategy only requires to annotate a part of label set given the selected samples and the remaining part can be inferred according to the learned label correlations. This strategy can effectively reduce the unnecessary annotation labor to construct the training set for a classifier. Specifically, we derive a multi-label Bayesian error bound and the new sample-label pairs are selected to minimize it.

Furthermore, we also develop an online adaptation model which update the existing model with only the newly-acquired samples. Most of the existing learning algorithm has to be retrained with all historically-acquired training samples. This learning scheme becomes impractical when more and more training samples are accumulated into the training set over time during the active learning iterations. Instead, the proposed online learner can efficiently update the existing model without retraining it. In detail, the new model is obtained by minimizing its Kullback-Leibler distance from the existing one under a set of multi-label constraints.

Finally, we conduct experiments on two benchmark data sets and a real-world image data set obtained from an image sharing website - Corbis. The experiments prove the superiority of the proposed 2DAL strategy to the other existing multi-label active learning algorithm. Furthermore, it also demonstrates the efficiency of the online learner compared to the other learning algorithm with retraining mode.

APPENDIX I
PROOF OF THE LEMMA 1

Here we give the proof of Lemma 1. *Proof:* Since the selected y_s can take on two values $\{0, 1\}$, there are two possible posterior distributions for the unlabeled y_i, i.e., $P\left(y_i|y_s = 0; y_{L(x)}, \boldsymbol{x}\right)$ and $P\left(y_i|y_s = 1; y_{L(x)}, \boldsymbol{x}\right)$. If $y_s = 1$ holds, the Bayesian classification error is [15]:

$$\begin{aligned}&\mathcal{E}\left(y_i|y_s = 1; y_{L(x)}, x\right) = \min\{P\left(y_i = 1|y_s = 1; y_{L(x)}, x\right)\\ &, P\left(y_i = 0|y_s = 1; y_{L(x)}, x\right)\}\end{aligned} \tag{47}$$

Given the inequality $\frac{1}{2}H(p) - \epsilon \leq \min\{p, 1-p\} \leq \frac{1}{2}H(p), \epsilon = \frac{1}{2}\log\frac{5}{4}$ (see figure 15), we have

$$\begin{aligned}&\tfrac{1}{2}H\left(y_i|y_s = 1; y_{L(x)}, \boldsymbol{x}\right) - \epsilon \leq \mathcal{E}\left(y_i|y_s = 1; y_{L(x)}, \boldsymbol{x}\right)\\ &\leq \tfrac{1}{2}H\left(y_i|y_s = 1; y_{L(x)}, \boldsymbol{x}\right)\end{aligned} \tag{48}$$

Similarly, if $y_s = 0$ holds,

$$\begin{aligned}&\tfrac{1}{2}H\left(y_i|y_s = 0; y_{L(x)}, \boldsymbol{x}\right) - \epsilon \leq \mathcal{E}\left(y_i|y_s = 0; y_{L(x)}, \boldsymbol{x}\right)\\ &\leq \tfrac{1}{2}H\left(y_i|y_s = 0; y_{L(x)}, \boldsymbol{x}\right).\end{aligned} \tag{49}$$

Therefore, the Bayesian classification error bound given the selected y_s can be computed as:

$$\begin{aligned}&\mathcal{E}\left(y_i|y_s; y_{L(x)}, \boldsymbol{x}\right)\\ &= P\left(y_s = 1|y_{L(x)}, \boldsymbol{x}\right)\mathcal{E}\left(y_i|y_s = 1; y_{L(x)}, \boldsymbol{x}\right)\\ &+P\left(y_s = 0|y_{L(x)}, \boldsymbol{x}\right)\mathcal{E}\left(y_i|y_s = 0; y_{L(x)}, \boldsymbol{x}\right)\\ &\leq \tfrac{1}{2}P\left(y_s = 1|y_{L(x)}, \boldsymbol{x}\right)H\left(y_i|y_s = 1; y_{L(x)}, \boldsymbol{x}\right)\\ &+\tfrac{1}{2}P\left(y_s = 0|y_{L(x)}, \boldsymbol{x}\right)H\left(y_i|y_s = 0; y_{L(x)}, \boldsymbol{x}\right)\\ &= \tfrac{1}{2}H\left(y_i|y_s; y_{L(x)}, \boldsymbol{x}\right)\end{aligned} \tag{50}$$

The last equality follows the definition of conditional entropy. And similarly

$$\begin{aligned}&\mathcal{E}\left(y_i|y_s; y_{L(x)}, \boldsymbol{x}\right)\\ &= P\left(y_s = 1|y_{L(x)}, \boldsymbol{x}\right)\mathcal{E}\left(y_i|y_s = 1; y_{L(x)}, \boldsymbol{x}\right)\\ &+P\left(y_s = 0|y_{L(x)}, \boldsymbol{x}\right)\mathcal{E}\left(y_i|y_s = 0; y_{L(x)}, \boldsymbol{x}\right)\\ &\geq \tfrac{1}{2}P\left(y_s = 1|y_{L(x)}, \boldsymbol{x}\right)\left\{H\left(y_i|y_s = 1; y_{L(x)}, \boldsymbol{x}\right) - 2\epsilon\right\}\\ &+\tfrac{1}{2}P\left(y_s = 0|y_{L(x)}, \boldsymbol{x}\right)\left\{H\left(y_i|y_s = 0; y_{L(x)}, \boldsymbol{x}\right) - 2\epsilon\right\}\\ &= \tfrac{1}{2}H\left(y_i|y_s; y_{L(x)}, \boldsymbol{x}\right) - \epsilon\end{aligned} \tag{51}$$

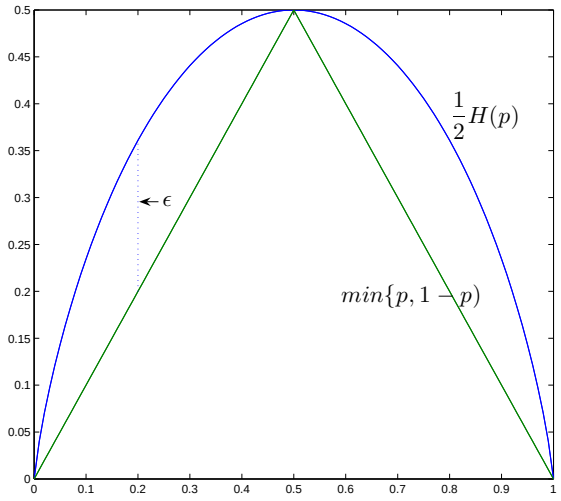

Fig. 15. Illustration of the inequality $\frac{1}{2}H(p) - \epsilon \leq \min\{p, 1-p\} \leq \frac{1}{2}H(p), \epsilon = \frac{1}{2}\log\frac{5}{4}$

■

REFERENCES

[1] L. Fei-Fei, R. Fergus, and P. Perona, "One-shot learning of object categories," *IEEE Transaction on Pattern Analysis and Machine Intelligence*, 2006.

[2] A. Kapoor, K. Grauman, R. Urtasun, and T. Darrel, "Active learning with gaussian processes for object categorization," in *Proc. of IEEE ICCV*, 2007.

[3] G.-J. Qi, X.-S. Hua, Y. Rui, J. Tang, T. Mei, and H.-J. Zhang, "Correlative multi-label video annotation," in *Proc. of ACM Conference on Multimedia (ACM Multimedia)*, 2007.

[4] S. Zhu, X. Ji, W. Xu, and Y. Gong, "Multi-labelled classification using maximum entropy method," in *Proc. of ACM SIGIR*, 2005.

[5] G.-J. Qi, Y. Song, X.-S. Hua, L.-R. Dai, and H.-J. Zhang, "Video annotation by active learning and cluster tuning," in *International Workshop on Semantic Learning Applications in Multimedia, in association with CVPR*, 2006.

[6] S. C. H. Hoi and M. R. Lyu, "A semi-supervised active learning framework for image retrieval," in *Proc. of IEEE CVPR*, 2005.

[7] A. Dong and B. Bhanu, "Active concept learning for image retrieval in dynamic databases," in *IEEE Proc. of ICCV*, 2003.

[8] R. Yan, J. Yang, and A. Hauptmann, "Automatically labeling data using multi-class active learning," in *Proc. of IEEE ICCV*, 2003.

[9] S. Tong and E. Y. Chang, "Support vector machine active learning for image retrieval," in *Proc. of ACM Conference on Multimedia*, 2001.

[10] E. Y. Chang, S. Tong, K. Goh, and C. Chang, "Support vector machine concept-dependent active learning for image retrieval," *IEEE Transaction on Multimedia*, 2005.

[11] A. Krause, A. Singh, and C. Guestrin, "Near-optimal sensor placements in gaussian processes: Theory, efficient algorithms and empirical studies," *Journal of Machine Learning Research*, vol. 9, pp. 235–284, 2008.

[12] X. Li, L. Wang, and E. Sung, "Multi-label svm active learning for image classification," in *Proc. of ICIP*, 2004.

[13] M. R. Boutell, J. Luo, X. Shen, and C. M. Brown, "Learning multi-label scene classification," *Pattern Recognition*, vol. 37, no. 9, 2004.

[14] K. Brinker, "On active learning in multi-label classification," *"From Data and Information Analysis to Knowledge Engineering" of Book Series "Studies in Classification, Data Analysis, and Knowledge Organization", Springer*, 2006.

[15] M. E. Hellman and J. Raviv, "Probability of error , equivocation, and the chernoff bound," *IEEE Transaction on Information Theory*, 1970.

[16] A. Kapoor and E. Horvitz, "On discarding, caching, and recalling samples in active learning," in *Proc. of Uncertainty and Artificial Intelligence*, 2007.

[17] F. Jing, M. Li, and H.-J. Zhang, "Entropy-based active learning with support vector machine for content-based image retrieval," in *Proc. of IEEE Conference on Multimedia and Expo*, 2004.

[18] N. Roy and A. McCallum, "Toward optimal active learning through sampling esitmation of error reduction," in *Proc. of ICML*, 2001.

[19] T. Cover and J. Thomas, *Elements of information theory, second edition*. New York: Wiley Series in Telecommunications, John Wiley and Sons, 2006.

[20] G.-J. Qi, X.-S. Hua, Y. Rui, J. Tang, and H.-J. Zhang, "Two dimensional active learning for image classification," in *IEEE Proc. of CVPR*, 2008.

[21] C. Bishop, *Pattern recognition and machine learning*. Springer, 2006, ch. Approximate Inference, pp. 461–473.

[22] S. F. Chen and R. Rosenfeld, "A gaussian prior for smooting maximum entropy models," School of Computer Science, Carnegie Mellon University, Tech. Rep. CMU-CS-99-108, 1999.

[23] J. Wu, X.-S. Hua, and B. Zhang, "Tracking concept drifting with gaussian mixture model," in *International Conference on Visual Communications and Image Processing*, 2005.

[24] D. C. Liu and J. Nocedal, "On the limited memory BFGS method for large scale optimization," *Mathematical Programming B*, vol. 45, no. 1-3, pp. 503–528, 1989.

[25] N. Syed, H. Liu, and K. Sung, "Incremental learning with support vector machines," in *Workshop on Support Vector Machines, at the IJCAI*, 1999.

[26] G. Cauwenberghs and T. Poggio, "Incremental and decremental support vector machine," in *Proc. of Neural Information Processing Systems*, 2000.

[27] J. Yang, R. Yan, and A. Hauptmann, "Cross-domain video concept detection using adaptive svms," in *ACM Conference on Multimedia*, 2007.

[28] A. P. Dempster, N. M. Laird, and D. B. Rubin, "Maximum-likelihood from incomplete data via em algorithm," *Journal of the Royal Statistical Society (Series B)*, vol. 39, no. 1, 1977.

[29] R. Neal and G. Hinton, *A view of the EM algorithm that justifies incremental, sparse, and other variants*, ser. Learning in Graphical Models, M. Jordan, Ed. Kluwer Academic Press, 1998.

[30] R. M. Neal, "Probabilistic inference using markov chain monte carlo methods," University of Toronto, Tech. Rep. CRG-TR-93-1, 1993.

[31] B. J. Frey and D. J. C. MacKay, "A revolution: belief propagation in graphs with cycles," in *Advances in Neural Information Processing Systems*, vol. 10. The MIT Press, 1998.

[32] T. Minka, "Expectation propagation for approximate bayesian inference," in *Proc. of the Seventeenth Conference on Uncertainty in Artificial Intelligence*, 2001.

[33] K. P. Murphy, Y. Weiss, and M. I. Jordan, "Loopy belief propagation for approximate inference: An empirical study," in *Proc. of Conference on Uncertainty in Artificial Intelligence*, 1999.

[34] T. Volkmer, J. R. Smith, and A. Natsev, "A web-based system for collaborative annotation of large image and video collections," in *Proc. of International ACM Conference on Multimedia*, 2005.

[35] A. Elisseeff and J. Weston, "A kernel method for multi-labelled classification," in *Proc. of NIPS*, 2002.

[36] L. Fei-Fei and P. Perona, "A bayesian hierarchical model for learning natural scene categories," in *Proc. of IEEE CVPR*, 2005.

[37] G.-J. Qi, X.-S. Hua, Y. Rui, J. Tang, Z.-J. Zha, and H.-J. Zhang, "A joint appearance-spatial distance for kernel-based image categorization," in *IEEE Proc. of CVPR*, 2008.

[38] B. Merialdo, J. Jiten, E. Galmar, and B. Huet, "A new approach to probabilistic image modeling with multimensional hidden markov models," in *Proc. of 4th International Workshop on Adaptive Multimedia Retrieval*, 2006.

[39] C. G. M. Snoek, M. Worring, J. C. Gemert, J.-M. Geusebroek, and A. W. M. Smeulders, "The challenge problem for automated detection of 101 semantic concepts in multimedia," in *Proceedings of the ACM International Conference on Multimedia*, Santa Barbara, USA, October 2006, pp. 421–430.

Guo-Jun Qi Mr. Guo-Jun Qi received the B.E. degree from University of Science and Technology of China in Automation, Hefei, Anhui, China, in 2005. His research interests include computer vision, multimedia, and machine learning, especially content-based image/video retrieval, analysis, management and sharing. He was the winner of the best paper award in the 15th ACM International Conference on Multimedia, Augsburg, Germany, 2007. He is now working in Internet Media Group at Microsoft Research Asia as a research intern. Mr. Qi is a student member of Association for Computing Machinery.

Xian-Sheng Hua Dr. Xian-Sheng HUA received the B.S. and Ph.D. degrees from Peking University, Beijing, China, in 1996 and 2001, respectively, both in applied mathematics. Since 2001, he has been with Microsoft Research Asia, Beijing, where he is currently a Lead Researcher with the internet media group. His current research interests include video content analysis, multimedia search, management, authoring, sharing and advertising. He has authored more than 130 publications in these areas and has more than 30 filed patents or pending applications. HUA is a member of the Association for Computing Machinery and IEEE. He is an adjunct professor of University of Science and Technology of China, and serves as an Associate Editor of IEEE Transactions on Multimedia and Editorial Board Member of Multimedia Tools and Applications. Hua won the Best Paper Award and Best Demonstration Award in ACM Multimedia 2007. He also won TR35 2008 Young Innovator Award of MIT Technology Review.

Yong Rui Dr. Yong Rui serves as Director of Strategy of Microsoft China R&D (CRD) Group. Before this role, Dr. Rui spent seven years and managed the Multimedia Collaboration team at Microsoft Research Redmond.

Dr. Rui is a Senior Member of both ACM and IEEE. He is an Associate Editor of ACM Transactions on Multimedia Computing, Communication and Applications (TOMCCAP), IEEE Transactions on Multimedia, and IEEE Tran on Circuits and Systems for Video Technologies. He was an Editor of ACM/Springer Multimedia Systems Journal (2004-2006), International Journal of Multimedia Tools and Applications (2004-2006), and IEEE Tran on Multimedia (2004-2008). He also serves on the Advisory Board of IEEE Transactions on Automation Science and Engineering. He received his BS from Southeast University, his MS from Tsinghua University, and his PhD from University of Illinois at Urbana-Champaign (UIUC). He also holds an Executive Training Certificate from Wharton Business School, University of Pennsylvania.

Dr. Rui contributes significantly to the research communities in computer vision, signal processing, machine learning, and their applications in communication, collaboration, and multimedia systems. His contribution to relevance feedback in image search created a new research area in multimedia. He has published twelve books and book chapters, and over seventy referred journal and conference papers. Dr. Rui holds 30 issued and pending US patents. Dr. Rui was on Organizing Committees and Program Committees of ACM Multimedia, IEEE CVPR, IEEE ECCV, IEEE ACCV, IEEE ICIP, IEEE ICASSP, IEEE ICME, SPIE ITCom, ICPR, CIVR, among others. He is a General Chair of Int. Conf. Image and Video Retrieval (CIVR) 2006, a Program Chair of ACM Multimedia 2006, and a Program Chair of Pacific-Rim Conference on Multimedia (PCM) 2006.

Jinhui Tang Dr. Jinhui Tang is currently a postdoctoral research fellow in School of Computing, National University of Singapore. He received his B.E. and PhD degrees in July 2003 and July 2008 respectively, both from the University of Science and Technology of China. From Jun. 2006 to Feb. 2007, he worked as a research intern in Internet Media group at Microsoft Research Asia. And from Feb. 2008 to May 2008, he worked as a research intern in School of Computing at National University of Singapore. He is a recipient of the 2008 President Scholarship of Chinese Academy of Science, and a co-recipient of the Best Paper Award in ACM Multimedia 2007. His current research interests include content-based image retrieval, video content analysis and pattern recognition. Dr. Tang is a member of ACM and a student member of IEEE.

Hong-Jiang Zhang Dr. HongJiang Zhang (M'91-SM'97-Fellow'03) received his Ph.D from the Technical University of Denmark, Lyngby in 1991 and his BS from Zhengzhou University, Henan, China, 1982, both in Electrical Engineering, respectively. From 1992 to1995, he was with the Institute of Systems Science, National University of Singapore, where he led several projects in video and image content analysis and retrieval and computer vision. From 1995 to 1999, he was a research manager at Hewlett-Packard Labs, Palo Alto where he was responsible for research and development in the areas of multimedia management and intelligent image processing. In 1999, he joined Microsoft Research, where he is currently the Managing Director of Advanced Technology Center in Beijing. Dr. Zhang is a Fellow of IEEE and ACM. He has co-authored/co-edited 4 books, over 350 papers and book chapters, numerous special issues of international journals on image and video processing, content-based media retrieval, and computer vision as well as over 60 granted patents. He currently serves as the Editor In Chief of IEEE Transactions on Multimedia and on the editorial board of Proceedings of IEEE.